Session A4:

DURABILITY OF CONCRETE WITH SUPPLEMENTARY CEMENTITIOUS MATERIALS (SCM)

SEM-EDS analysis of products formed under natural and accelerated carbonation of concrete with CEM I, CEM II/B-M and CEM II/B-V

Andres Belda Revert*
PhD student
e-mail:
andres.b.revert@ntnu.no

Mette Rica Geiker*
PhD, Professor
e-mail:
mette.geiker@ntnu.no

Klaartje De Weerdt*
PhD, Associate Professor
e-mail:
klaartje.d.weerdt@ntnu.no

*
Norwegian University of Science and Technology (NTNU),
Department of Structural Engineering
Richard Birkelands vei 1 A, 7491. Trondheim

Ulla Hjorth Jakobsen
PhD, Senior Consultant
Danish Technological Institute (DTI)
Concrete Centre
Gregersensvej 4, DK 2630 Taastrup
e-mail: uhj@teknologisk.dk

ABSTRACT
Carbonation resistance of concrete is usually tested under accelerated conditions, i.e. by elevating the CO_2 concentration compared to natural conditions and keeping the RH close to 60%. However, it is not clear if these conditions mirror the natural process. Using SEM-EDS we investigated the composition of the reaction products of carbonated and non-carbonated concrete containing 0, 18 and 30% fly ash exposed to three different carbonation conditions. In non-carbonated concrete the reaction products depended on the binder. However, in carbonated concrete the reaction products were similar in composition in all the concretes and exposure conditions tested.

Key words: Carbonation, Supplementary Cementitious Materials (SCM), Testing

1. INTRODUCTION

Carbonation is a spontaneous reaction of the cement paste with the CO_2 present in the atmosphere. It is a slow process under natural conditions (0.03% CO_2) and is therefore accelerated for testing purposes by controlling the relative humidity (50-65%) and using increased CO_2 concentration (e.g. 1 to 50%, see summary in [1]). Carbonation causes changes in microstructure, phase composition and pH of the pore solution in the cement paste [2]. It is, however, not clear if the accelerated exposure conditions cause similar changes compared to natural carbonation.

The investigation is part of a PhD study on carbonation-induced corrosion in fly ash concrete. In the project two different accelerated conditions were used in addition to natural conditions: one to accelerate carbonation (60% RH and 1% CO_2) and one where also corrosion in carbonated concrete is facilitated (90% RH and 5% CO_2). The aim of the investigation is to check if the tested accelerated conditions mirror the natural carbonation process. The phase composition, pore solution and other microstructural features in the carbonated concrete, especially in the vicinity of the reinforcement, will influence reinforcement corrosion. In this paper, we focus on the composition of the reaction products.

2 EXPERIMENTAL

Concretes containing three different cements water-to-binder ratio 0.54-0.56 and 370 kg/m^3 cement were prepared. The cements contained limestone addition (4%) and different amounts of fly ash CEM I (0%), CEM II/B-M (18%) and CEM II/B-V (30%), see Table 1. The concrete samples were kept in the mould for three days and when demoulded wrapped in plastic for 11 days. After this period, they were carbonated for 20 weeks. Three exposure conditions were used: "N": natural carbonation sheltered from rain, "1-60": 60% RH and 1% CO_2, and "5-90": 90% RH and 5% CO_2. The temperature was in all cases close to 20ºC. Polished epoxy impregnated sections were prepared at the Danish Technological Institute (DTI). All polished sections were carbon coated before testing. A scanning electron microscope Quanta 400 ESEM from FEI operated at high vacuum mode, accelerating voltage of 15 kV, spot size 5 and working distance of around 10 mm was used. The data was Proza corrected. 50 points were manually taken selecting the outer reaction products in carbonated ("Carb") and non-carbonated ("Non") areas of each sample.

3 RESULTS AND DISCUSSION

Figure 1 presents the data obtained by SEM-EDS point analysis. The horizontal axis shows the Si/Ca molar ratio and the vertical the Al/Ca molar ratio. The ideal stoichiometry of the following phases is indicated: calcium hydroxide (CH) and calcium carbonate (C$\underline{\text{C}}$) in the origin, and on the vertical axes ettringite (AFt) and monosulphate (AFm). The estimated composition of the C-S-H for the tested non-carbonated concretes is marked with large black squares. During the SEM-EDS point analysis a certain volume is analysed, which generally includes a mixture of phases and the resulting point lies in between the ideal stoichiometry of the phases in the mixture. The points taken in the non-carbonated areas indicate the presence of AFm, AFt, CH/C$\underline{\text{C}}$ and C-S-H. In the carbonated areas less AFm and AFt phases seem to be present as fewer points are found between the C-S-H and AFt or AFm compositions. The points associated with C-S-H in the carbonated concrete seem to gather mainly around a Si/Ca ratio from 0.15-0.35. This is opposite of what one would expect. Upon carbonation C-S-H decalcifies [3] and one would expect the data point to move to higher Si/Ca ratios. A possible reason for the observation is that during SEM-EDS point analysis a volume comprising several phases is analysed. The lower Si/Ca ratio may originate from fine intermixing of decalcified C-S-H and C$\underline{\text{C}}$. This is in line with recent TEM observations indicating the formation of finely dispersed C$\underline{\text{C}}$ crystals in C-S-H upon carbonation [4].

Table 1 – Chemical composition of the cements determined by XRF [% by mass]

Cement	Label	SiO_2	Al_2O_3	Fe_2O_3	CaO	MgO	SO_3	P_2O_5	K_2O	Na_2O
CEM I	A	20.4	4.8	3.4	61.7	2.2	3.5	0.2	0.9	0.5
CEM II/B-M	B	27.5	8.4	3.9	52.7	1.6	2.6	0.2	0.6	0.5
CEM II/B-V	C	29.5	10.8	4.5	44.6	2	3.2	0.4	1.1	0.5

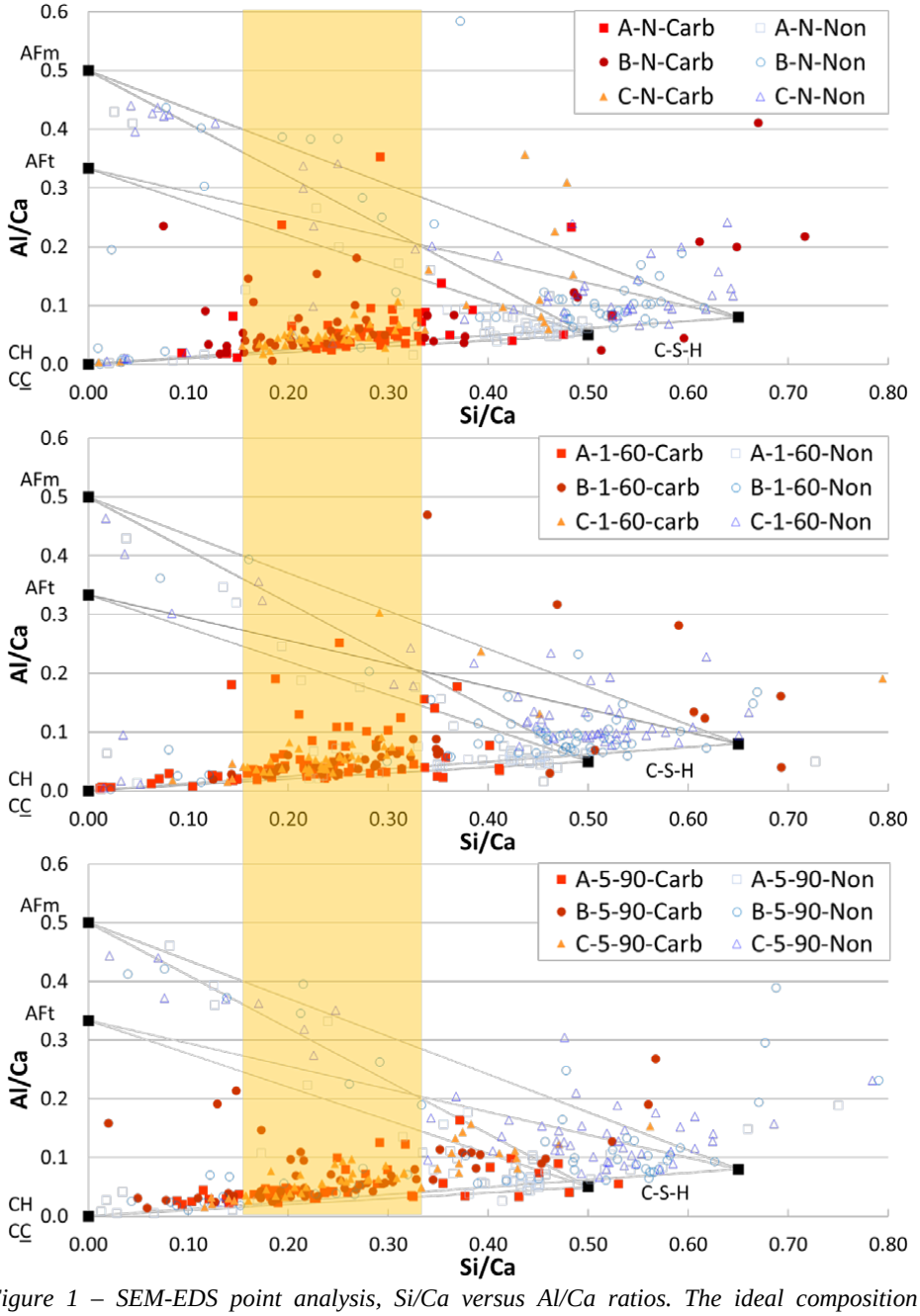

Figure 1 – SEM-EDS point analysis, Si/Ca versus Al/Ca ratios. The ideal composition of ettringite (AFt), monosulphate (AFm), portlandite (CH) and calcium carbonate (C$\underline{C}$), as well as the estimated compositions of C-S-H in the non-carbonated concretes with fly ash (Si/Ca=0.65) and without fly ash (Si/Ca=0.5) are marked. The shaded area indicates the data points in carbonated concrete (0.15-0.35 Si/Ca) where decalcified C-S-H is finely intermixed with C$\underline{C}$.

The lowering of the Si/Ca ratio of C-S-H related points upon carbonation indicates that Ca redistributes in the system. For example, Ca originating from portlandite will dissolve and precipitate as very small CC crystals finely intermixed with the decalcified C-S-H. Note that a mass balance of the Ca cannot be performed as only few manually selected points were analysed. Similar observations using SEM-EDS point analysis on mortars containing similar binders exposed to 60% RH and 1% CO_2 were reported earlier [5]. The results presented in this paper show that upon carbonation decalcified C-S-H is finely intermixed with CC independently of the binder as well as the exposure conditions. As the reaction products are in equilibrium with the pore solution, the results indicate that the composition of the pore solutions upon carbonation might not be that different either. Assuming similar pore structure, it could lead to comparable concrete resistivity in carbonated concrete. Further research is needed to confirm this.

5 CONCLUSION

Concretes with varying fly ash content were exposed to natural and accelerated carbonation and the reaction products were investigated using SEM-EDS. The data shows that the reaction products upon carbonation are similar for the tested concretes and exposures conditions even if the initial hydration products were different.

AKNOWLEDGEMENTS

The current paper is part of a larger research project 'Lavkarbsem' (NFR project no. 235211/O30). The project is supported by the Norwegian Research Council and the following companies, Engineering AS, HTC (Heidelberg Technology Center), Mapei AS, Norbetong AS, Norcem AS, Rambøll AS and Skanska AS.

REFERENCES

[1] Harrison, T., Jones, M., Newland, M. Kandasami, S. and Khanna, G. “Experience of Using the prTS 12390-12 Accelerated Carbonation Test to Assess the Relative Performance of Concrete.” Magazine of Concrete Research 64 (8): 737–47 (2012)

[2] Bertolini, L., Elsener, B., Pedeferri, P., Redaelli, E. and Polder, R.: “Corrosion of Steel in Concrete”, Wiley-VCH Verlag GmbH & Co, Weinheim, Germany, pp. 79-91 (2013)

[3] Sevelsted, T. F. and Skibsted, J.: “Carbonation of C–S–H and C–A–S–H samples studied by ^{13}C, ^{27}Al and ^{29}Si MAS NMR spectroscopy”, Cement and Concrete Research, Vol. 71, pp. 56-65 (2015)

[4] Herterich, J., Black, L. and Richardson, I.: “Microstructure and phase assemblage of low-clinker cements during early stages of carbonation”, 14th International Congress on the Chemistry of Cement, Beijing, China (2015)

[5] Revert, A. B., De Weerdt, K., Hornbostel, K. and Geiker, M.R.: “Investigation of the effect of partial replacement of Portland cement by fly ash on carbonation using TGA and SEM-EDS”, International RILEM Conference on Materials, Systems and Structures in Civil Engineering, Lyngby, Denmark, pp. 413-422 (2016)

On the porosity development in cement pastes containing slag: Influence of curing conditions and the effect of carbonation.

Monica Lundgren
M.Sc., Tek. Lic., researcher
Research Institutes of Sweden RISE, Built Environment
CBI Cement and Concrete Research Institute
Brinellgatan 4, SE-504 62 Borås
e-mail: monica.lundgren@ri.se

Arezou Babaahmadi
M.Sc., PhD., researcher
Research Institutes of Sweden RISE, Built Environment
CBI Cement and Concrete Research Institute
Brinellgatan 4, SE-504 62 Borås
e-mail: arezou.babaahmadi@ri.se

Urs Mueller
M.Sc., PhD., senior researcher
Research Institutes of Sweden RISE, Built Environment
CBI Cement and Concrete Research Institute
Brinellgatan 4, SE-504 62 Borås
e-mail: urs.mueller@ri.se

ABSTRACT
The study presented has focus on the pore structure development in cement pastes containing ground granulated blast furnace slag and the effect of carbonation. The topic is relevant for better understanding, and for dealing with, the higher vulnerability of slag-containing concretes to carbonation and its impact on the freeze-thaw scaling. The issue of curing conditions prior to carbonation is approached. Prolonged sealed curing without carbonation leads to a pore refinement and lowered total pore volume in all blends, but exposure to carbonation from 28 days has a different effect, depending on the slag content of the blend and on the curing regime.

Key words: Cement, Carbonation, Supplementary Cementitious Materials (SCM), Granulated Blast furnace Slag (GBS), Porosity, Pore structure.

1. INTRODUCTION

With the growing volumes of concrete used in construction worldwide we also witness a growing awareness for the environmental impact involved, in particular for the need to reduce the emissions of CO_2 associated to the cement production. However, while the use of supplementary cementitious materials (SCM) has become rather widespread, we still do not have sufficient knowledge to safely predict how concretes with the new blended binders will behave in the long run. While we know that e.g. the use of ground granulated blast furnace slag (GBS) leads to mitigation of alkali-silica reactions or increased resistance to sulphate attack, we do not understand exactly why, or to what extent, nor do we know the exact cement substitution level by slag that would place the concrete on the safe side for 25 years or more.

Slag is also known to make concrete vulnerable to carbonation and to freeze-thaw attack. While carbonation leads to reduced porosity and reduced scaling for concrete with OPC it has an opposite effect for a concrete with slag. Carbonation in binder blends with slag increases the porosity and leads to higher scaling upon frost attack. Information on how the porosity or microstructure develops at earlier hydration stages provides valuable guidance for durability estimations. The pore evolution in an aging concrete, however, will always depend on the precise aging conditions, which may differ from a zone closer to the surface, to a zone in the inner part of a large element. Laboratory results are also strictly related to the specific curing conditions adopted. The study below shows an attempt to approach the issue of curing and the effect on the pore structure in carbonating cement pastes.

2 DESCRIPTION OF THE STUDY

The study presented here focuses on the effect of carbonation on blends with slag. The pore structure was analysed by mercury intrusion porosimetry (MIP). It is part of a series of projects carried out at CBI on hydration and durability of concrete with SCM in binary or ternary blends.

2.1 Materials and mixtures

The binders are shown in Table 1. Experiments were carried out on cement pastes with water-binder ratio 0.45, labelled after the binder code in Table 1.

Table 1 – The blended binders used in the study (values in mass-% of total amount of binder).

	CEM I 42.5 RR[a]	CEM II/B-M (S-LL) 42.5[b]	GBS1[b]
C (Ref)	100		
S		100[c]	
S1	70		30
S2	50		50

a) Norway b) Sweden c) S-LL: 16% GBS1-6% Limestone

2.3 Experimental set-up

Cement pastes were cast in polyethylene bottles (Ø ~ 63 mm, H ~125 mm), tightly sealed after casting. The experiments were carried out at 20 °C. Prior to the carbonation tests the pore structure has been analysed on non-carbonated pastes through hydration tests under continuous sealed conditions; see Fig. 1, left, (details are found in [1]). For the carbonation tests, specimens were produced by cutting the PE bottles in two halves, transversely to the height, and the cut surface was used as test surface in the carbonation tests (Fig. 1, right). The specimens were

exposed to accelerated carbonation from the age of 29 days: unidirectional diffusion, 1 % CO_2 at 65 % relative humidity (RH). Up to 28 days the specimens had been subjected to different curing: *standard*, as the conditions in most European standards for concrete testing, or *sealed*, to mimic a curing regime attained in protected inner parts of a concrete element.

- *Standard*: 1 day in PE bottle then demoulded and cut, stored 6 days in water and 21 days at 65 % RH. Coated at day 28, using two-component epoxy resin, all sides except test surface.
- *Sealed*: 28 days in the bottles and then cut. Coated as above.

3 RESULTS AND DISCUSSION

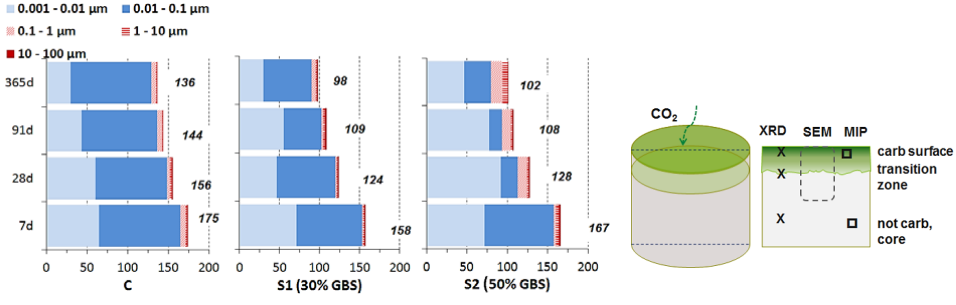

Figure 1 – Left: total pore volume (mm^3/g) and distribution by pore radius intervals after hydration in sealed conditions to indicated age (from [1]). Right: sketch of the carbonation test.

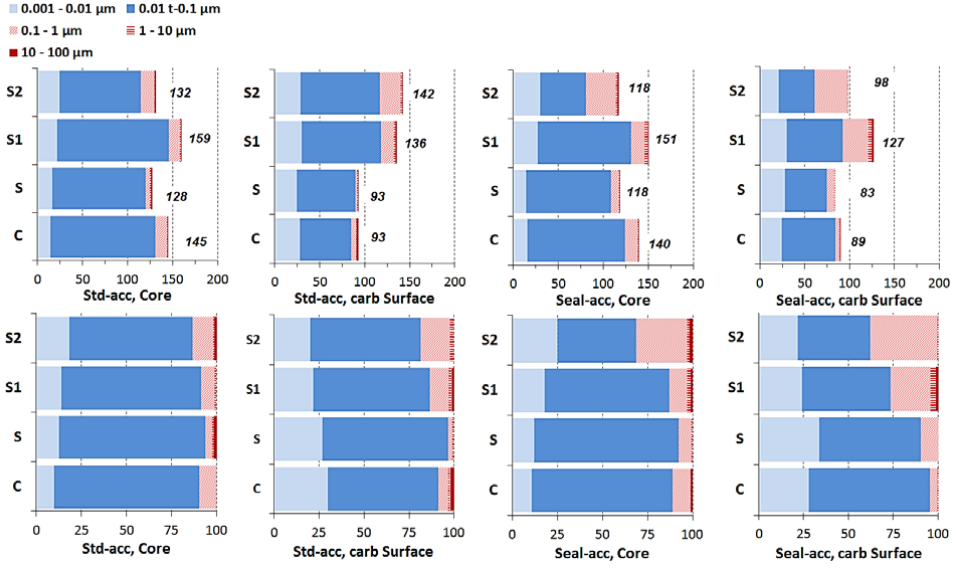

Figure 2 – Results from accelerated carbonation. Upper: total pore volume (mm^3/g) and distribution by pore radius intervals. Lower: distribution as % of the total pore volume. Each bar shows smallest radii to the left, highest to the right.

Figure 1 shows that with continuous sealed curing (hydration) in all pastes the total pore volume decreased with curing/ hydration time. At the same age, from 28 days and on, the total pore volume in pastes with slag was lower (S1, S2 vs. C). However, even if S1 and S2 developed similar total pore volumes, a higher volume of small pores (radii 0.001-0.01 μm) could be observed in S2 (with higher slag content) compared to S1. With increasing curing time, C showed no pore refinement towards smaller pores but S1 and S2 did up to 91 days. After that the pore structure coarsened slightly at 365 days. The shift towards coarser pore sizes is more visible in S2, probably due to autogenous shrinkage and micro-cracking, observed also by [2].

Figure 2 shows a summary from the carbonation test. Specimens were analysed after 32 weeks of carbonation. During the test a drying and carbonation shrinkage (micro-) cracking has been observed, in all pastes but more pronounced in S1 and S2. This has undoubtedly affected the progress of carbonation. Portlandite and the calcium silicate hydrates (C-S-H) are affected differently by the CO_2; consequently the carbonation of the two will have a different effect on the developed pore system. By powder X-ray diffraction (XRD) the calcite polymorphs vaterite and aragonite were observed in the top carbonated layer of all pastes, indicating advanced stages of carbonation and start of the decalcification(-shrinkage) of C-S-H (see further [3],[4]). Higher slag content, hence more magnesium in S2, also promoted formation of more aragonite, a denser polymorph with smaller molar volume than that of calcite or vaterite. These comments explain briefly that if pore "clogging" can often occur in carbonated OPC pastes (mainly from calcite having higher molar volume than the portlandite) this is obviously less likely to occur in pastes with high slag content, with less portlandite and a C-S-H with lower Ca/Si ratio. The latter having a higher potential for decalcification shrinkage and cracking.

The results show that C, S, and to a smaller extent also S1, acquired a lower total pore volume in the carbonated surface layer compared to the un-carbonated core. In C and S a higher fraction of fine pores (radius 0.001-0.01 μm), is seen. This is also true for S1 but here also the fraction of larger pores (radius 0.1-1 μm) increased at carbonation, particularly in S1-seal. For S2, the total pore volume seems to be more or less the same in the carbonated vs. un-carbonated zone, standard or sealed. In S2-seal, however, the total pore volume is almost equally divided between three intervals, 0.001-0.01, 0.01-0.1, 0.1-1 μm, even in the un-carbonated zone. The reason is still to be clarified; to this point we only know that in the un-carbonated zone more hydrotalcite has formed in S2-seal compared to S2-std (hence more slag had reacted), but also more portlandite. In S1-seal vs. S1-std this difference was less noticeable.

REFERENCES

[1] Mueller, U., Lundgren, M., Malaga, K.: "Development of pore structure and hydrate phases of binder pastes blended with slag, fly ash and metakaolin. A comparison", 14th International Congress on the Chemistry of Cement, Beijing, China (2015)

[2] Canut M.M.: "Pore structure in blended cement pastes". PhD thesis, Department of Civil Engineering, Technical University of Denmark (2011).

[3] Chen, J.J., Thomas, J.J., Hamlin M. Jennings, H.M.: "Decalcification shrinkage of cement paste", Cement and Concrete Research, vol. 36, pp. 801-809, (2006)

[4] Morandeau, A., Thiéry, M., Dangla, P.: "Investigation of the carbonation mechanism of CH and C-S-H in terms of kinetics, microstructure changes and moisture properties", Cement and Concrete Research, vol. 56, pp 153-170, (2014)

Durability of slag blended binder systems towards sulphate ingress

Arezou Babaahmadi
M.Sc., Ph.D.,
CBI Cement and Concrete Research institute
Box 857, 50115 Borås
e-mail: Arezou.babaahmadi@ri.se

Monica Lundgren
M.Sc., Tek Lic.,
CBI Cement and Concrete Research institute
Box 857, 50115 Borås
e-mail: Monica.Lundgren@ri.se

Urs Mueller
M.Sc., Ph.D.,
CBI Cement and Concrete Research institute
Box 857, 50115 Borås
e-mail: Urs.Mueller@ri.se

ABSTRACT
This paper describes results of an investigation on the sulphate resistance of slag blended binder pastes and mortar specimens over a period of 1 year. The focus is on showing the importance of the chemistry of components when discussing sulphate resistance and the relation of that to the hydrate phase assemblage. Moreover the importance of the test method for evaluations is pointed out.

Key words: Cement, Supplementary Cementitious Materials (SCM), Testing

1. INTRODUCTION

1.1 General

This paper describes partial outcomes of a study which focuses on sulphate attack in blended binders, which can be important in subterranean environments and even under fresh and seawater conditions. Sulphate attack manifests in the field through decreased performances of the exposed structure, which is characterised by a loss in strength due to cracking, de-cohesion and softening of the cementitious matrix. The focus in this paper is the sulphate ingress and resistance of slag blended binder pastes and mortar specimens over a period of 1 year.

2. MATERIALS AND METHODS

The materials, which were procured and used for the study are CEM I 42.5 RR (**C**), CEMII/B-M 42.5 (**S**) and slag from a Swedish producer. The blended binder systems are CEM I + 30 % slag (**S1**) and CEM I + 50 % slag (**S2**). All the systems have w/b ratio of 0.5.

2.2 Sulphate ingress tests

Sulphate ingress tests were performed in a 30 g/l sulphate solution. In the case of sulphate immersion tests for pastes, samples were prepared in a standard Hobart blender by mixing dry powder together with water. The fresh pastes were transferred to polyethylene (PE) bottles. The bottles were stored for 28 days in a climate-controlled chamber (20 °C, 50% RH). Afterwards, the specimens were cut into two equal pieces and placed in a 30 g/l solution, as shown in Figure 1. In the case of mortar bars, dry powder was mixed together with water and standard sand (0/2) for mortar preparation according to EN 196-1, and cast in a form especially made for preparation of six flat prisms with a size 10 x 40 x 160 mm^3, to be further used in expansion measurements. The test was performed according to a German test method (SVA).

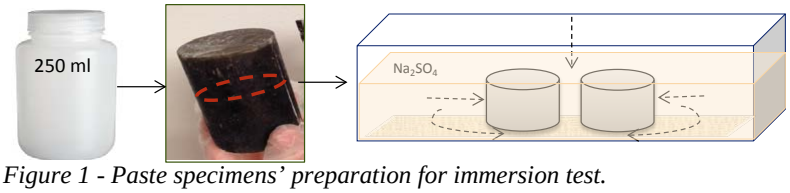

Figure 1 - Paste specimens' preparation for immersion test.

3. RESULTS

3.1 Paste specimens

The frequent visual changes due to sulphate ingress in paste specimens after 6 and 12 month is presented in Figure 2. As shown, both reference (C) and Slag containing series (S, S1 and S2) are indicating extreme surface damage due to sulphate ingress. The surface damage in 1 year exposed slag containing samples was to the extent that further profiling was completely impossible. Sulphur profiles from elemental mapping, which was performed by micro X-ray fluorescence analysis, is presented in Figure 3. An approximate damage zone illustrates the lost parts of the ingress profiles due to extreme surface damage. It can be seen that the slag containing series are showing much higher sulphate intrusion compared to the reference samples. Furthermore, the X-Ray Diffraction (XRD) analysis results on the ingress zone of paste specimens after 6month of sulphate intrusion are presented in Figure 4 (left). As can be seen both Ettringite and Gypsum peaks are extremely high in Slag containing samples.

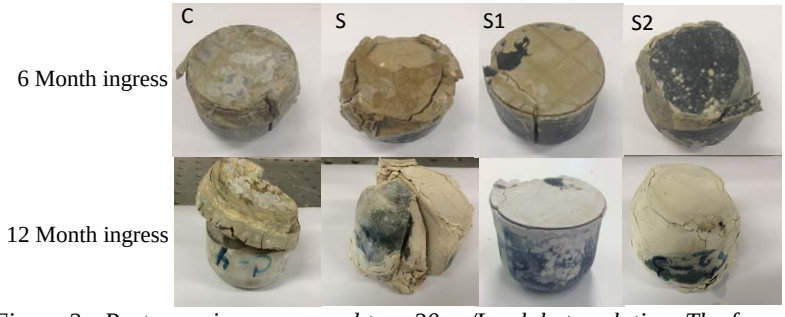

Figure 2 - Paste specimens exposed to a 30 gr/L sulphate solution. The frequent damages after 6 and 12 month are presented.

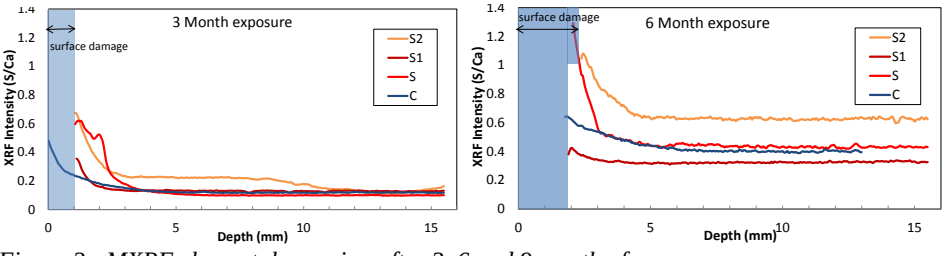

Figure 3 - MXRF elemental mapping after 3, 6 and 9 month of exposure.

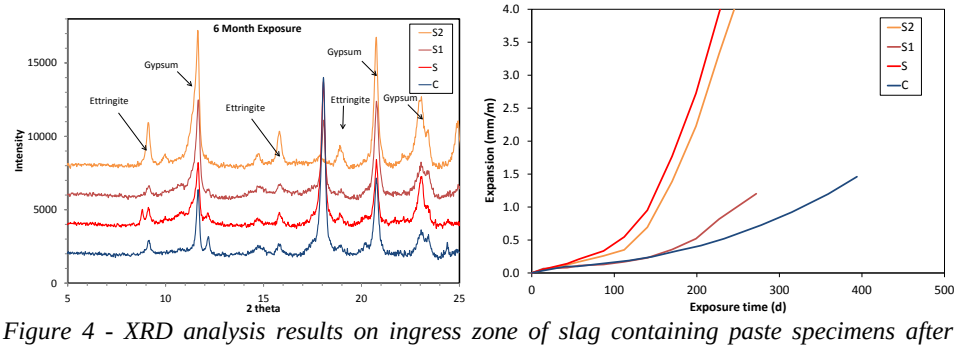

Figure 4 - XRD analysis results on ingress zone of slag containing paste specimens after 6 month of sulphate intrusion (left). Immersion test results for mortar flat prisms stored in a 30 g/l sulphate solution (right).

3.2 Mortar bars

The immersion test results for the mortar bars are presented in Figure 4 (right). The results are in accordance with the outcomes of the immersion test for paste specimens. As shown the expansion in slag containing samples are much higher than that of the reference samples.

4 DISCUSSION

There exists a general belief concerning slag containing binder systems, which indicates that due to a finer pore structure in these systems, a better resistivity towards sulphate ingress is expected. However, this study shows, that not only the pore structure plays a role but the chemistry of the components and the resulting hydrate phase assemblage are important parameters to be considered. In Figure 5, the hydrate phase assemblage of the slag containing

binder systems is presented for up to 1 year of hydration under sealed conditions (no sulphate ingress). As shown, all binders are indicating production of monosulphate while ettringite occurs in minor amounts. This can largely be due to low sulphate content in the system which can also be seen from the calorimetry curves presented in Figure 6, were the sulphate depletion point is marked. This has caused stability of monosulphate and massive production of ettringite when sources of sulphates were introduced to the system, which was confirmed with our study.
The test method prescribes a threshold value of 0.5 ‰ of expansion after 91 days. Accordingly all binders would have passed the test. Figure 5 illustrates, however, that a drastic increase in expansion is possible just after 100 days.

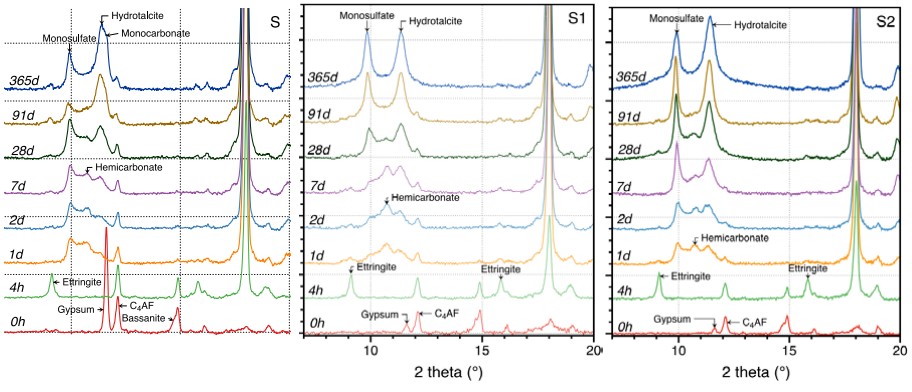

Figure 5 - X-Ray Diffraction analysis results for the S, S_1 and S_2 binder systems.

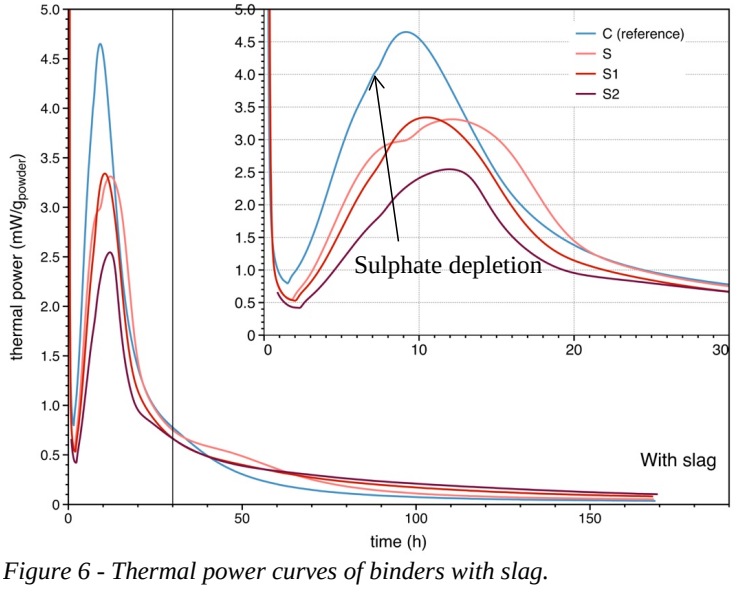

Figure 6 - Thermal power curves of binders with slag.

Durability testing of low clinker binders - chloride ingress in similar strength mortars exposed to seawater

Mette Rica Geiker, M.Sc., Ph.D. Professor,
Department of Structural Engineering, Norwegian University of Science and Technology, NO-7491 Trondheim,
Visiting Professor, Department of Civil Engineering, Technical University of Denmark, Brovej 118, DK-2800 Kgs. Lyngby,
e-mail: mette.geiker@ntnu.no

Klaartje De Weerdt
M.Sc., Ph.D., Associate Professor
Department of Structural Engineering, Norwegian University of Science and Technology, NO-7491 Trondheim, Norway
e-mail: klaarte.d.weerdt@ntnu.no

Sergio Ferreiro Garzón
M.Sc., Ph.D., Chemical Engineer
Research and Development Center, Cementir Holding S.p.A. Aalborg Portland, 9220 Aalborg, Denmark
e-mail: sergio.f.garzon@aalborgportland.com

Mads Mønster Jensen
M.Sc., Ph.D.
Dept. of Civil Engineering, Technical University of Denmark, Brovej 118, DK-2800 Kgs. Lyngby, Denmark
e-mail: mmoj@byg.dtu.dk

Björn Johannesson
M.Sc., Ph.D., Professor
Department of Building Technology, Linnæus University
e-mail: bjorn.johannesson@lnu.se

Alexander Michel
M.Sc., M.Sc., Ph.D., Assistant Professor
Dept. of Civil Engineering, Technical University of Denmark, Brovej 118, DK-2800 Kgs. Lyngby, Denmark
e-mail: almic@byg.dtu.dk

ABSTRACT
Resistance to chloride ingress of ten different binders was investigated. Most of the binders were prepared with 35% substitution of a new clinker by limestone filler, calcined clay, burnt shale and/or siliceous fly ash. Mortar samples with similar design compressive strength after 90 days were exposed to artificial sea-water for 270 days. The results indicate that the use of alternative binders may lead to up to around 15% reduction in CO_2 emission without compromising 90 days compressive strength and resistance to chloride ingress in marine exposure.

Key words: Cement, Chlorides, Supplementary Cementitious Materials (SCM)

1. INTRODUCTION

It is well known that cement production is responsible for around 5% of the total anthropogenic CO_2 emissions. Reduced clinker content is generally associated with lower CO_2 emission. The purpose of this paper is to investigate the resistance to chloride ingress of low clinker binders in similar strength mortars. Well hydrated mortars were exposed to seawater for 270 days and chloride profiles were determined by profile grinding and titration.

2. EXPERIMENTAL

Total chloride profiles were measured on mortar samples which were cast, cured and analysed according to procedures reported recently [2]. The chemical compositions of the binder constituents determined by XRF are given in Table 1. The binder compositions are given in Table 2. These binder compositions include hemihydrate, which is excluded when calculating clinker replacement according to EN 197-1 [1]. A binder composition typical for a Danish ready-mixed concrete for aggressive environments and strength class C35 was used as reference. The mortar compositions are given in Table 3. The mortars were designed to have similar compressive strength at 90 days; this led to variation in w/b. The mix design was based on 90 days compressive strength data according to EN 196-1 [3] (Table 2) and Bolomey's equation [4]. The paste volume was kept constant, and the SP content was adjusted to obtain fresh mortar flow comparable to the reference (R1). The CO_2 emissions per ton of binder (Table 3) were estimated considering hemihydrate, fly ash and burnt shale as CO_2 neutral, and assuming 0.85 t CO_2/t of clinker, 0.1 t CO_2/t of limestone filler, and 0.27 t CO_2/t of calcined clay. The CO_2 reductions were calculated considering the CO_2 emissions from each constituent and the w/b variations. Mixing was undertaken according to EN 196-1 [3], except that the mixing procedure was adjusted to include the delayed addition of a polycarboxylate ether based superplasticizer (SP). The mortar was cast in 125 ml plastic bottles (ø 50.5 mm). A small amount of water was added on top of the mortar to ensure saturated conditions. After 90 days curing, approximately 5 mm was cut from the bottom surface and the remaining surfaces were sealed by epoxy. The samples were re-saturated and finally exposed to artificial seawater with a composition according to ASTM D1141-3 [5]. Twelve samples were submerged in 2.5 L. The exposure solution was exchanged after 14 and 28 days and thereafter every 30 days. After 270 days of exposure, chloride ingress was determined by profile grinding and titration.

Table 1 - Chemical composition of binder constituents (main oxides) in [%] by mass.

	RAPID	Clinker in RAPID	New clinker	Calcined clay	Limestone filler	Burnt Shale	Fly ash
SiO_2	19.4	20.2	19.5	62.5	12.7	34.2	55.0
Al_2O_3	5.4	5.5	6.1	16.6	3.6	8.2	19.9
Fe_2O_3	3.8	4.0	3.3	9.4	1.8	4.8	5.5
CaO	63.2	65.4	66.0	0.8	44.0	30.1	4.5
MgO	0.94	0.80	0.92	2.95	0.60	5.59	1.81
K_2O	0.34	0.54	0.52	2.82	0.58	4.38	2.16
Na_2O	0.26	0.21	0.25	1.95	0.23	0.11	1.12
SO_3	3.4	1.5	1.6	0.4	0.4	5.6	0.4
LOI	2.6	0.24	0.47	2.39	35	4.55	3.2

Table 2 - Binder compositions in [%] by mass and mean and standard deviation of compressive strength at 90 days [MPa] determined in mortar according to EN 196-1 (w/b=0.5), but normalized to 2% air content.

id	Fly ash	New clinker	Hemi-hydrate	RAPID	Burnt shale	Calcined clay	Limestone filler	90 days strength
R1	16.7			83.3				67.9 ± 0.9
B1	16.7	76.5	2.8				4.0	67.2 ± 2.3
B2	18.2	63.7	2.3				15.8	62.1 ± 1.5
B3	18.2	63.7	2.3				15.8	64.5 ± 1.1
B4	19.0	63.7	1.5		7.9		7.9	67.2 ± 0.7
B5	19.4	63.7	1.1		11.9		4.0	66.3 ± 2.0
B6		63.7	2.3				34.0	58.2 ± 1.4
B7		63.7	2.3			25.5	8.5	79.3 ± 2.8
B8		63.7	2.3			34.0		71.6 ± 0.9
B9	7.5	58.9	2.2			15.7	15.7	72.0 ± 1.5

Table 3 – Mortar compositions (adjusted to same compressive strength) and CO_2 emission. The calculated CO_2 reductions combine the impact of binder composition and w/b.

id	Binder [g]	SP [g]	Demineralized water [g]	Sand [g]	w/b [-]	CO_2 [t/t binder]	CO_2 reduction [%]
R1	450.0		225.0	1350	0.50	0.65	0
B1	452.6		224.5	1350	0.50	0.65	0
B2	464.2	1.02	216.3	1350	0.47	0.56	13
B3	456.8	0.59	219.2	1350	0.48	0.56	14
B4	448.8	0.83	222.0	1350	0.50	0.55	17
B5	451.7	1.35	220.7	1350	0.49	0.55	17
B6	482.9	1.79	213.3	1350	0.44	0.58	6.2
B7	416.7	0.45	233.1	1350	0.56	0.62	13
B8	434.2	2.37	224.2	1350	0.52	0.63	7.2
B9	433.6	0.38	226.2	1350	0.52	0.56	18

3. RESULTS AND DISCUSSION

Chloride ingress profiles after 270 days exposure to seawater of mortars with comparable design compressive strength at 90 days are shown in Figure 1. The maximum total chloride concentration is found at a depth of approximately 2-3 mm for all mortar samples, while a decreased total chloride concentration is observed at the surface. The effect is explained by leaching and other phase changes causing a reduced binding capacity, see e.g. [6,7]. The ingress depths are comparable for all binders, expect for the binder with 34% limestone filler (B6), which exhibited a very low ingress resistance. The alternative binders appear to exhibit a higher total chloride content, indicating an increased binding capacity compared to the reference blend (R1). Furthermore, the beneficial impact of calcined clay (B7-B9) is illustrated in Figure 1 (right). The binding capacity for these blends is increased while the ingress depth is decreased, compared to the binder with only limestone filler (B6). The observations are in agreement with earlier findings, see e.g. [8].

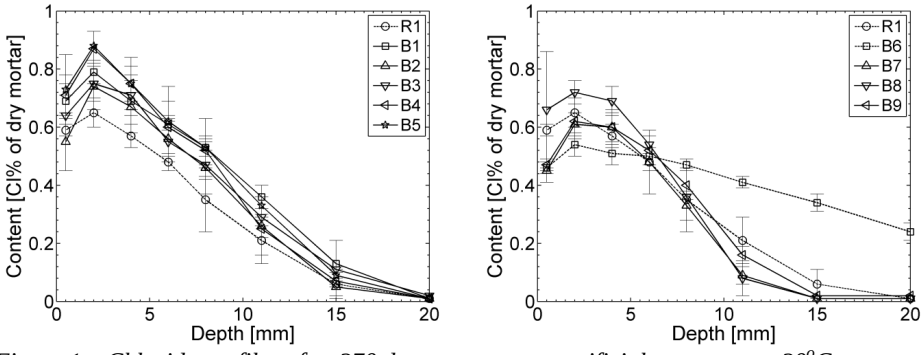

Figure 1 – Chloride profiles after 270 days exposure to artificial sea water at 20°C.

4. CONCLUSIONS

Based on the present investigation and assumptions, up to around 15% reduction in CO_2 emission from binder production might be obtained for selected binders without compromising the 90 days compressive strength and resistance to chloride ingress in marine exposure by using alternative binders instead of a binder composition typical for a Danish ready-mixed concrete for aggressive environments and strength class C35. Due to varying degree of reaction at testing the long-term chloride resistance needs to be documented. Other issues to be considered are e.g. carbonation resistance and conditions for reinforcement corrosion.

ACKNOWLEDGEMENTS

The work was undertaken as part of the project "Green transition of cement and concrete production" ("Grøn Beton II"). The financial support from the Danish Innovation Fond (InnovationsFonden) and the contribution from project partners are acknowledged.

REFERENCES

[1] DS/EN 197-1 4 ed., Cement – Part 1: composition, specification and conformity criteria for common cements, The Danish Standards Association (2012)

[2] De Weerdt, K., Geiker, M.R., "Comparing chloride ingress in Portland cement based binders with slag or fly ash exposed to seawater and deicing salt". In preparation (2017)

[3] DS/EN 196-1, Method of testing cement – Part 1: Determination of strength. The Danish Standards Association (2005)

[4] A. D. Herholdt, C. F. P. Justesen, P. N. Christensen, A. Nielsen. Beton-Bogen, Cementfabrikkernes tekniske oplysningskontor, Aalborg Portland, 2nd edition (1985). ISBN 87-980916-0-8.

[5] ASTM D1141 – 98, standard practice for the Preparation of Substitute Ocean Water, 1998 (2013)

[6] De Weerdt, K., Orsakova, D., Muller, A.C.A, Larsen, C.K, Pedersen, B.; Geiker, M.R., "Towards the understanding of chloride profiles in marine exposed concrete, impact of leaching and moisture content". Construction and Building Materials. vol. 120, (2016)

[7] Jakobsen, U.H., De Weerdt, K., Geiker, M.R., "Elemental zonation in marine concrete", Cement and Concrete Research. vol. 85 (2016)

[8] Shi, Z., Geiker, M.R., Lothenbach, B., De Weerdt, K., Ferreiro Garzón, S. Enemark-Rasmussen, K., Skibsted, J., "Friedel's salt profiles from thermogravimetric analysis and thermodynamic modelling of Portland cement-based mortars exposed to sodium chloride solution", Cem. Concr. Compos. vol. 78, pp. 73 - 83 (2017)

Carbonation of concrete with mineral additions

Helén Jansson, Assistant Professor
Chalmers University of Technology, 412 96 Gothenburg

Robin Snibb, M.Sc.
Master student (2016) Chalmers University of Technology

Karl Bohlin, M.Sc.
Master student (2016) Chalmers University of Technology

Ingemar Löfgren, PhD
Thomas Concrete Group AB, 412 54 Gothenburg
ingemar.lofgren@thomasconcretegroup.com

ABSTRACT
This study investigated how mineral addition, fly ash and slag (GGBS), influences carbonation, and how carbonation affects chloride migration and transport properties in mortar. Accelerated carbonation, Rapid Chloride Migration (RCM), capillary absorption tests (NT Build 368) and compressive strength tests (SS-EN 196-1) were conducted in a comparative study of mortar mixtures with different levels of mineral addition and *w*/*b* ratios. Carbonation rate increased and compressive strength was reduced with increased amount of mineral addition. The results also showed an interdependence between different deteriorating processes. Carbonation reduced the porosity, rate of reaching saturation and connectivity of the pore structure.

Key words: Carbonation, Supplementary Cementitious Materials (SCM), Testing.

1. INTRODUCTION

Porosity affects the rate of deterioration, by influencing the diffusion of CO_2 during carbonation and the ingress of chlorides. Generally, reduced total porosity leads to less connectivity between the capillary pores, which decrease permeability and penetration of chlorides and the rate of CO_2-diffusion. From a durability point of view, there is a critical value of capillary porosity around 25%, above which the permeability increases significantly. The increase in permeability consequently increases capillary absorption, through which water containing chlorides and CO_2 can penetrate. Both the capillary porosity and the pore size decrease by decreased *w*/*b* ratio and increased degree of hydration. According to Nagala & Page [1] carbonation reduces the total porosity, in both PC concrete and concrete with mineral additions, but with a redistribution of the pore size, showing a slight increase of the proportion of large capillary pores (diameters above 30 nm) in PC concretes and a significant increase in blended concretes. This effect is caused by the reduction of hydration products, e.g. calcium hydroxide, as a result of the larger volume in the formation of $CaCO_3$ (Dyer 2014). A study carried out by Wu & Ye [2] did however show that cement pastes containing high levels of mineral additions increases porosity. This is explained by an increase in porosity when C-S-H is carbonated, while carbonation of $Ca(OH)_2$ decreases porosity. As mineral additions contain less $Ca(OH)_2$ compared to Portland cement, which explains differences in porosity-change after carbonation between concretes with high and low amount of mineral addition. This paper presents the result from a master thesis [3] where the relative carbonation resistance of different binders (CEM I, fly ash and GGBS) was investigated and how carbonation effect transport properties, capillary absorption and chloride migration. The results for chloride migration is presented in [3].

2. EXPERIMENTAL PROGRAMME

The test program is based on the test matrix presented in Table 1 showing the *w*/*b* ratios, type of cement and amount of mineral addition. All tests were carried out on mortar specimens mixed with sea sand from Denmark, sieved to sieve-size < 2 mm.

Table 1. Investigated binder mixes (GGBS and Fly ash amount of total binder content).

Cement	GGBS / Fly ash	*w*/*b*
CEM I 42.5 N SR 3 MH/LA	0 %	0.40, 0.50, 0.60
CEM I 52.5 N	0 %	0.40, 0.50, 0.60
CEM I 52.5 N	20 % & 35 % FA	0.40, 0.50, 0.60
CEM I 52.5 N	35 %, 50 % & 65 % GGBS	0.40, 0.50, 0.60

For all the investigated binder mixes in Table 1, the compressive strength and the carbonation depth and rate were determined. For the carbonation tests the specimens were water cured for 7 days and then stored at 65 % RH (20°C) until 28 days age, where after they were placed in a CO_2-chamber with 2.0 % CO_2 and 65 % RH (20°C) and exposed for 7 weeks. Prior to CO_2 exposure, two side faces of the prisms (top and bottom) were coated to prevent carbonation. For the mixes with *w*/*b* 0.50 capillary absorption tests (NT Build 368) [4] and Rapid Chloride Migration tests (NT Build 492) [5] were conducted on un-carbonated and partially carbonated specimens (due to time limitations). Hence, the carbonated specimens were not homogenous in this respect which needs to be considered when comparing the results.

3. RESULTS AND DISCUSSION

In Figure 1 the carbonation rate (calculated from 2.0% to 0.04% CO_2) has been plotted against the compressive strength for all binder mixes. What can be seen from Figure 1 is that at lower amounts (20 % FA and 35 % GGBS) the effect on compressive strength and carbonation rate is not that large, but at higher dosage rates the effect is more substantial and that the effect of 35 % fly ash corresponds to 50 % GGBS.

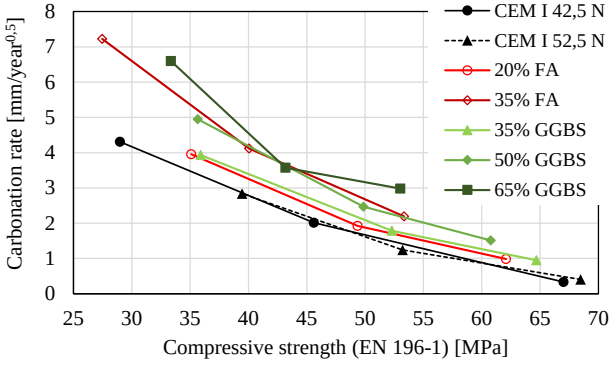

Figure 1. Carbonation rate (calculated to a CO_2 concentration of 0.04 %) versus compressive strength.

In Table 2 the calculated k-values based on compressive strength and on carbonation rate is presented, the calculation is based on the principle introduced by Smith [6]. The calculated *k*-values for strength is higher than for those based on carbonation. With respect to carbonation, all

mixes except the one with 35 % fly ash have a *k*-value higher than the prescribed value in EN 206 [7]. It should be noted that the accelerated testing on the mixes with higher amounts of fly ash and slag are more negatively affected by an accelerated carbonation test due to the slower and lower degree of hydration when starting the test compared to a natural exposure.

Table 2. Calculated k-values based on strength and carbonation resistance.

Mix	***k*-value strength**	***k*-value carbonation**	**Prescribed *k*-value (EN 206)**
20 % Fly ash	0.73	0.58	0.4
35 % Fly ash [i)]	0.55	0.25	(0.4)
35 % GGBS	0.96	0.81	0.6
50 % GGBS	0.92	0.75	0.6
65 % GGBS [ii)]	0.81	0.65	(0.6)

i) In EN 206 the maximum amount of fly ash to be taken into account is 25 % (fly ash/cement ≤ 0.33).
ii) In EN 206 the maximum amount of GGBS to be taken into account is 50 % (GGBS/cement ≤ 1.0)

In Figure 3 the results from the capillary absorption tests are presented, please not that these tests were conducted on un-carbonated and partially carbonated specimens (due to time limitations). The capillary absorption coefficient k_{cap} (or inverse of this, $1/k$) is shown in Figure 3(a) and in Figure 3(b) the capillary absorption resistance m_{cap} is presented. The coefficients are determined as:

$$k_{cap} = \frac{Q_{cap}}{\sqrt{t_{cap}}} \quad [\mathrm{kg/(m^2\sqrt{s})}] \tag{1}$$

where Q_{cap} is the absorbed water ($\mathrm{kg/m^2}$) and t_{cap} is the time to completion of capillary absorption (s).

$$m_{cap} = \frac{t_{cap}}{h^2} \quad [\mathrm{s/m^2}] \tag{2}$$

where h is the thickness of the specimen (m).

As can be seen in Figure 2, carbonation leads to a decreased capillary absorption coefficient ($1/k_{cap}$ increases) and increased capillary absorption resistance (m_{cap} increases), the only exception is the mix with 65 % GGBS. The effect is more significant for the specimens with CEM I, and in particular the CEM I 42.5 N SR3 MH/LA). These changes, decreased k_{cap} and increased m_{cap}, indicate that the porosity is reduced as a result of carbonation. It was also found that all the carbonated mortars showed a reduction in total open porosity, see [3]. Fly ash mortars showed the greatest decrease in total open porosity, with increasing porosity-reduction by increasing amount of mineral addition. GGBS mortars, on the other hand, showed a peak in porosity-reduction at 50% GGBS.

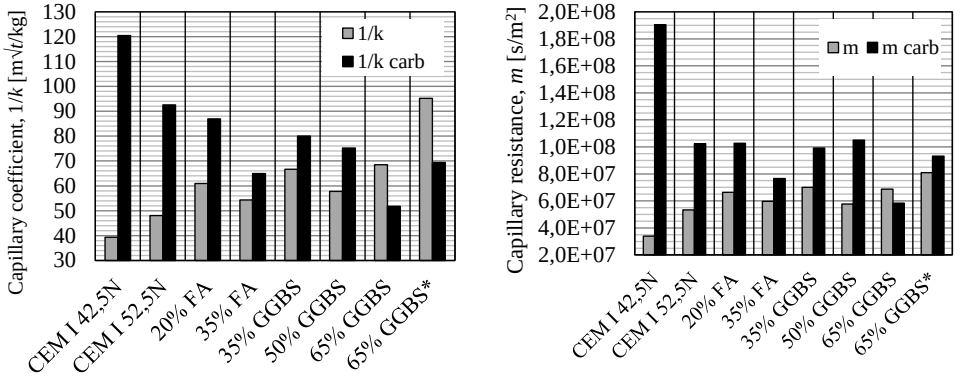

(a) *(b)*

Figure 2. Effect of carbonation on (a) the inverse capillary coefficient (1/k) and (b) the capillary resistance. For 65% GGBS the fineness was increased from Blaine 420 m^2/kg to 520 m^2/kg.*

4. CONCLUSIONS

Based on the result of this study, the following conclusions can be made:

- In the accelerated carbonation tests (2.0 % CO_2) the carbonation rate increased with mineral additions. But at moderate amounts (up to 20 % fly ash and 50 % GGBS) the effect was moderate and when comparing with the mixes made of CEM I 42.5 N SR MH/LA the carbonation rate was only slightly higher.
- The calculated *k*-values based on compressive strength was higher when based on carbonation. The calculated *k*-values were however higher than the ones prescribed in EN 206 [7], the only exception being the *k*-value for carbonation for the mix with 35 % fly ash.
- The capillary absorption tests on carbonated and un-carbonated specimens showed that the porosity was reduced by carbonation, with the exception of the mix with 65 % GGBS.

REFERENCES

[1] Nagala, V T., & Page, C L., Effects of Carbonation on Pore Structure and Diffusional Properties of Hydrated Cement Pastes. *Cem. and Conc. R.* vol. 27, issue 7, pp. 995-1007.

[2] Wu, B., & Ye, G., *Development of porosity of cement paste blended with supplementary cementitious materials after carbonation*. 14th International Congress of the Chemistry of Cement; 13-16 October 2015, Beijing. pp. 1-18.

[3] Bohlin, K., & Snibb, R., *Carbonation of concrete - Effect of mineral additions and influence on transport properties*. Master's Thesis BOMX02-16-42, Chalmers University of Technology.

[4] NT Build 368, *Concrete, repair materials: Capillary Absorption*. Espoo, Nordtest, 1991.

[5] NT Build 492, *Concrete, mortar and cement-based repair materials: Chloride migration coefficient from non-steady-state migration experiments*. Espoo, Nordtest, 1999.

[6] Smith, I.A., *Design of fly ash concretes*. Proc Inst Civil Eng 1967;36:769–90.

[7] EN 206, *Concrete - Specification, performance, production and conformity*. CEN, 2013.

The influence of low chloride migration in concrete with mineral addition on minimizing climate impact of bridges

Nadia Al-Ayish
M.Sc., Ph.D. candidate
CBI Cement and Concrete Research Institute
Drottning Kristinas v. 26, 114 28 Stockholm
e-mail: nadia.al-ayish@ri.se

Otto During
M.Sc.
CBI Cement and Concrete Research Institute
Drottning Kristinas v. 26, 114 28 Stockholm
e-mail: otto.during@ri.se

Katarina Malaga
M.Sc., Ph.D., associate professor
CBI Cement and Concrete Research Institute
Drottning Kristinas v. 26, 114 28 Stockholm
e-mail: katarina.malaga@ri.se

ABSTRACT
In order to reach a specific service life of concrete structures a certain coverage thickness is needed. At present, this is regulated with national requirements which besides a minimum cover thickness also puts constrains on mineral addition in different environment exposures. Latest studies show, however, that this cover thickness does not match reality and that mineral addition should be taken into consideration as well. In this study a LCA was performed on a bridge where the climate impact is calculated according to the latest research on chloride induced corrosion. The concrete was mixed with different amounts of mineral addition and the results were compared with the national regulations.

Key words: Corrosion, Supplementary Cementitious Materials (SCM), Sustainability, climate impact, bridge, chloride migration, durability, service life.

1. INTRODUCTION

There is a need to reduce the climate impact of the built environment. Alongside with international and national regulations Swedish Transport Administration (Trafikverket) has set a vision to reduce the climate impact of infrastructures by 15 % until 2020, 30 % until 2025 and zero emission by 2050, compared to levels from 2015. To reach this vision Trafikverket has since 2016 put a demand that all infrastructure projects with an investment cost above 50 million SEK (approximately 5 million euros) have to declare their climate impact [1]. Concrete is the most common material used for construction of bridges in Sweden [2]. Due to that fact, optimisation of concrete will have a big part in reducing the environmental impact.

One way to reduce the environmental impact of concrete structures is by resource efficiency. Ordinary Portland cement (OPC) is the major contributor to the environmental impact and a decrease can be achieved by minimizing the share of OPC through the use of supplementary cementitious materials (SCM) from industrial by-products or by not using an overly strong concrete. Another CO_2 reducing action is by making the construction durable with a longer service life and less maintenance.

Chloride induced corrosion is one of the main durability problems in concrete structures in the world [3]. Due to the cold climate, the long costal line and the use of de-icing salts, the frost- and chloride attack are the most common durability problems of reinforced concrete (RC) structures in Sweden [4]. At present, the durability and service life of RC structures is mainly based on regulations which besides a minimum cover thickness also puts constrains on mineral addition in different environment exposures. Latest studies show, however, that this cover thickness does not match reality and that mineral addition should be taken into consideration as well [5]. Tang [5] suggests an overall higher cover thickness especially for concrete with OPC thus resulting in an increased volume of concrete.
The aim of this research is to investigate the environmental consequence of recent studies of durability of different mineral additions compared to today's regulations. It also aims to suggest an approach to implementing sustainability with durability. A life cycle assessment (LCA) of five mix designs with various amounts of mineral additions was performed and implemented on a bridge edge beam exposed to de-icing salt. The study does not only consider the climate impact of the materials but also the effect on the durability.

2. METHOD

2.1 Life cycle assessment

The climate impact of concrete exposed to chlorides was evaluated through a LCA approach which considers both the materials and the technical service life.
The concrete was analysed in three steps:

1. Calculation of global warming potential (GWP) per cubic meter of mix design.
2. Application of the concrete mixes in a bridge edge beam with a cover thickness according to the regulations and the recent study. The bridge edge beam is 10 meter long with 4 wt% reinforcement.
3. The durability aspects were considered where the service life is calculated according to two models on chloride ingress.

2.2 Concrete mixes

Five different concrete mix designs with a constant water-binder ratio at 0.40 are compared, Table 1. Mix 2 contains no mineral addition while the other mixes contain different amounts of mineral addition. While mixes 1-3 and 5 have mineral addition values that are acceptable for frost resistance according to SS 137003, the Swedish application of EN 206, mix 4 has a ground-granulated blast-furnace slag (GGBS) that exceeds the limit [6]. However, recent studies showed that a GGBS content of up to 40 % is reasonable with respect to the salt-frost scaling resistance [7]. Although this is outside the governing regulations this is still an interesting aspect to include.

Table 1 – Mix design

Mix	w/b	OPC	Fly ash	GGBS
1	0.40	353	69	
2	0.40	425		
3	0.40	340		85
4	0.40	302		123
5	0.40	350	87.5	

2.3 Service life prediction

The service life of the bridge edge beam is based on figures from [5], which use the ClinConc model, and calculations using the simple ERFC model, which is based on Fick's second law of diffusion. No age factor has been considered. The service life difference between concrete with two different cover thicknesses using the ERFC model is expressed in equation (1).

$$t_1 = t_2 * \left(\frac{x_1}{x_2}\right)^2 \quad (1)$$

Where:

$t_{1\ and\ 2}$ = service life of concrete 1 and 2 [year]

$x_{1\ and\ 2}$ = cover depth of concrete 1 and 2 [mm]

According to [5] concrete with OPC which is exposed to de-icing salt needs a concrete cover of 70 mm to be able to reach a service life of 100 years. When adding mineral additions the concrete cover can be reduced to 45 mm. This can be compared with the regulations which have a minimum cover thickness of 45 mm regardless of mineral addition.

3. RESULTS AND DISCUSSION

Following today's standard on minimum cover thickness the results showed a decrease of 23 % when comparing mix 2 with mix 4 during the material production stage, Figure 1. Adopting the proposed cover thickness would in this case increase the GWP of OPC due to the extra volume of material. Although the difference between the OPC concrete and the SCM concrete would be bigger, a 38 % decrease could be made just by adding 16 % Fly ash (FA). When including the durability aspect the results would be more dramatic. A small increase in concrete volume leads to a significant decrease in GWP. Not only does FA and GGBS concrete have a lower chloride migration, but many researches also demonstrated that the durability improves over time due to the aging of the material [8].

These results are achieved with a concrete that has a water-binder ratio at 0.40. Similar results would be achieved with a water-binder ratio at 0.45 but the amount of mineral addition and cover thickness that is needed for a 100 year lifetime would be a bit different. This shows the importance of including the durability aspects and the actual concrete performance when optimizing the GWP of a concrete structure. The durability is not only important for the climate impact but also for maintenance planning and life cycle cost analysis. The whole life cycle should be included in the analysis when optimizing the concrete.

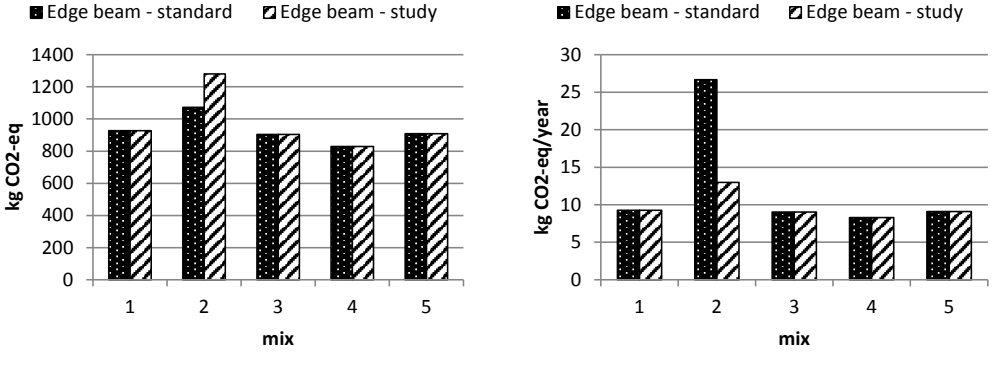

Figure 1 - GWP of the bridge edge beam during material production (left) and service life (right). Concrete cover in today's standard is compared with proposed concrete cover.

4. CONCLUSIONS

Based on the research of [5] the consequence of adopting the proposed cover thicknesses into the application standard EKS 10 [9] would lead to a decrease of GWP to least 50 % regarding the bridge edge beam with OPC. Having cover thicknesses that depend on mineral addition would push the industry towards a more sustainable development and an increased demand for use of FA and GGBS.

In addition to including mineral addition in the application standard, Trafikverket should also, with regard to this research, push the sustainable development forward by adding a limit for minimum amount of mineral addition in concrete structures exposed to chlorides.

Durability and technical service life should be included when optimizing concrete structures based on environmental impact. Performing a LCA based on the design service life today could give misleading results.

ACKNOWLEDGEMENT

This study was financed by SBUF and the CBI Foundation.

REFERENCES

[1] Trafikverket: ”Klimatkrav i byggprojekt - ett viktigt steg mot klimatneutral infrastruktur”, http://www.trafikverket.se/om-oss/nyheter/Nationellt/2016-02/klimatkrav-i-byggprojekt---ett-viktigt-steg-mot-klimatneutral-infrastruktur/

[2] Du, G.: ”Life cycle assessment of bridges, model development and case studies”, Doctoral Thesis, KTH Royal Institute of Technology. (2015)

[3] Luping, T., Utgennant, P., Boubitas, D.: “Durability and Service Life Prediction of Reinforced Concrete Structures”, Journal of the Chinese Ceramic Society, Vol 43 (2015)

[4] Racutanu, G.: “The Real Service Life of Swedish Road Bridges - A Case Study”. Doctoral thesis. KTH Royal Institute of Technology. (2001)

[5] Luping, T., Löfgren, I.: “Evaluation of Durability of Concrete with Mineral Additions with regard to Chloride-Induced Corrosion”, Report No. 2016-4, Chalmers University of Technology, Gothenburg, Sweden (2016)

[6] SS 137003:2015: “Concrete – Application of SS-EN 206 in Sweden”, Swedish Standards Institute (2015)

[7] Löfgren, I., Esping, O., Lindvall, A.: ” The influence of carbonation and age on salt frost scaling of concrete with mineral addition”, International RILEM Conference on Materials, (2016)

[8] Shi, X,. Xie, N., Fortune, K., Gong, J.: “Durability of steel reinforced concrete in chloride environments: An overview”, Construction and Building Materials, pp 125-138 (2012)

[9] Boverket: “Boverkets byggregler, EKS 10”, Boverket (2016)

Session A5:

CARBONATION, CHLORIDE INGRESS AND CORROSION

Evaluation after 17 years of field exposures on cracked steel fibre reinforced shotcrete

Erik Nordström
Ph.D., Adjunct Professor
KTH Royal Institute of Technology
Division of Concrete Structures
SE-100 44 STOCKHOLM, Sweden
e-mail: erik.nordstrom@byv.kth.se

ABSTRACT
Evaluation of a long-term field exposure of cracked steel fibre reinforced shotcrete samples show degradation of the load-bearing capacity due to corrosion on steel fibres in the cracks. Especially for samples exposed to de-icing salts. Crack width rules the time for initiation but only show a limited influence on the corrosion rate. Longer fibres corrode faster due to the larger cathode area. To conclude it can be stated that it is not realistic to expect a service-life of 100 years with remained load-bearing capacity in the tested chloride exposed environments.

Key words: Shotcrete, Cracking, Carbonation, Chlorides, Corrosion, Fibres, Reinforcement.

1. INTRODUCTION

1.1 General

Since the 1980s reinforcement of shotcrete with steel fibres has been common practice in rock support. Crack width distribution in service limit state and residual strength in ultimate limit state are the advantages from use of fibres. Civil structures with steel fibre reinforced shotcrete (SFRS) have service-life requirements beyond 100 years and thereby the risk for, and the effect on load bearing capacity from a potential steel fibre corrosion in cracked SFRS is of interest. Previous evaluations have been presented [1, 2, 3] and here an evaluation from 17 years of exposure.

1.2 Scope and goal

The scope of the field exposures is to study if, and under what circumstances, steel fibre corrosion is initiated in cracked shotcrete in common environments. The goal with the field exposures are:

- Define time to initiation and corrosion rate after any initiation.
- Investigate influence from relevant parameters on the corrosion process.
- Study long term influence on residual strength capacity with ongoing corrosion

2 METHODOLOGY

In the following section the set-up for the field exposures is described.

2.1 Shotcrete types and mixes

Both wet-mix and dry-mix shotcrete samples have been used in the field exposures. At the time when the exposures were designed the most commonly used accelerator for wet-mix shotcrete

was sodium silicate based ones (water glass). In addition, many civil structures have been constructed with shotcrete containing water glass. The dominating steel fibre types was a low carbon steel fibre with end-hook, commonly 30 or 40 mm long. The SFSR-samples were pre-cracked to 0.1, 0.5 and 1.0 mm before exposure.

2.2 Exposures sites

The samples have been exposed in three different environments that is considered typical for SFRS (see table 1 below).

Table 1 – Exposure environment.

	Exposure type	Corresponding Structure
Eugenia tunnel	- Humid, sheltered from rain - Chlorides from de-icing salts - Exhausts - Frost	- Rock support in tunnels
Motorway RV40	- Humid and exposed for rain - Chlorides from de-icing salts - Exhausts - Frost	- Rock support in open cuts - Concrete repair
River Dalälven	- Humid and exposed for rain - Frost - Flowing river water - Ice erosion	- Intake channels & tunnels to hydropower plants

2.3 Evaluation methods

Corrosion attack

Evaluation of the corrosion is done by measuring the fibre diameter in the part (corroded) crossing the crack. To decompose the SFSR and collect the fibres crossing the crack a five-step method was developed. Briefly the concrete samples were cut in 20 mm slices at three levels from the crack mouth. Thereafter the slices were dried before completely saturated with water by vacuum treatment. The saturated samples were exposed to a repeated freeze-thaw cycle until the concrete matrix is pulverized and the unaffected fibres were collected with a magnet. The amount of corrosion is expressed as loss of cross sectional area in comparison with the original area.

Residual load-bearing capacity

After exposure of the SFSR-samples (500*125*75 mm) they were exposed to reload in the laboratory. Two different approaches for evaluation of the change in load-bearing capacity was developed. 1. Direct comparison – Comparison of the end load level before exposure with the load level after exposure. 2. Statistical comparison - Comparison between the load level at 2 mm deformation after exposure with the statistically expected level before exposure (at 2 mm).

Chloride content & Carbonation

A chloride profile from the surface and at different depths along the crack surface was measured with the RCT-method. Carbonation was detected with phenolphthalein solution.

3 RESULTS

Results from the evaluation of data after 17 years contains all exposure sites. The data from motorway Rv40 has been reprocessed with the new evaluation approach. (Data from 10 years).

3.1 Corrosion attack

The detection of corrosion is depending on the fact that a corroded sample must be found to be able to make the measurement. The process (sawing, decompose the concrete matrix etc.) gives a risk for rupture of corroded fibres. This is a major drawback with the methodology. A ruptured fibre will not be able to be detected. In figure 1 below an example of results is shown for the standard mix (wet-mix with 30 mm fibres, w= 0.5 mm, WA30) that is available on all exposure sites. The corrosion attack was initiated already after 1 year at the most severe exposure for de-icing salts at RV40 and after 10 years also in mild exposure in the river Dal. Deeper down in the crack corrosion also initiates with time. In figure 2 the effect of fibre length can be seen. As can be seen the time for initiation is longer at river Dal but the attack is almost similar after time. At both RV40 and in river Dal the longer fibres in average corrode faster. For Rv40 the rate seems to decline at 10 years, but probably this is since the evaluation methodology will not make it possible to find very heavily corroded fibres. Therefore, the tests at Rv40 was finalized.

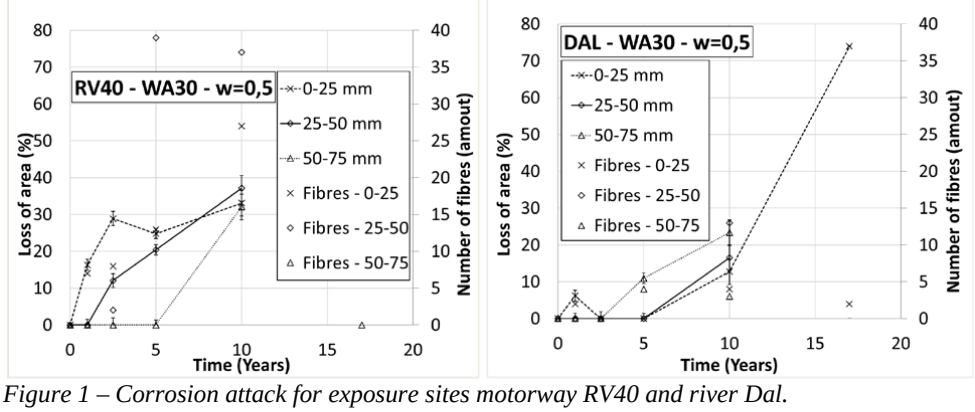

Figure 1 – Corrosion attack for exposure sites motorway RV40 and river Dal.

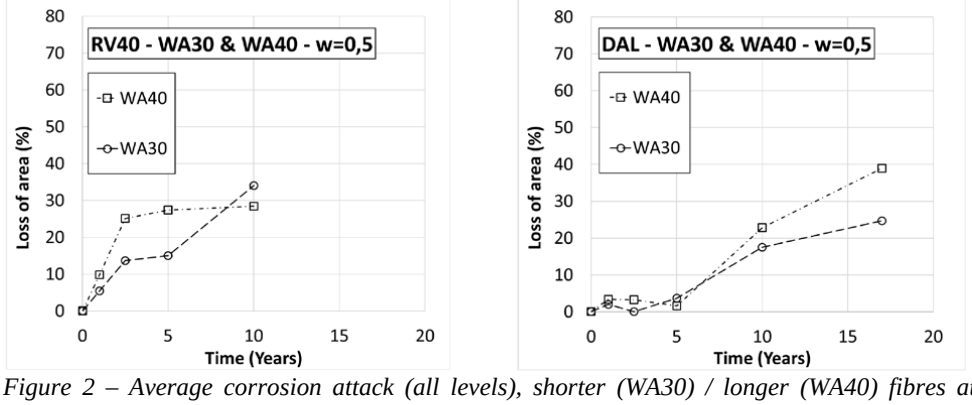

Figure 2 – Average corrosion attack (all levels), shorter (WA30) / longer (WA40) fibres at motorway RV40 and river Dal.

3.2 Residual load-bearing capacity

The impact on the residual load-bearing capacity is obvious for samples with initiated corrosion, especially at deformations up to 2 mm. In figure 3 an example from motorway RV40 is shown.

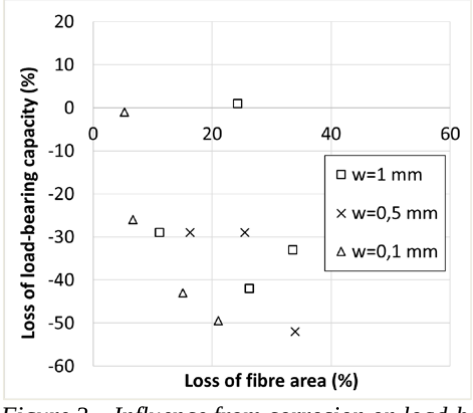

Figure 3 – Influence from corrosion on load-bearing capacity at 2 mm deformation for exposure sites motorway RV40, WA30 samples (Statistical evaluation).

4 CONCLUSIONS

All samples show steel fibre corrosion after 17 years of exposure. The attack is most severe at Rv40 that is an environment with a combination of high level of humidity and high exposure to de-icing salts. Most accentuated influence from mix-type was seen in samples with longer steel fibres that corroded much faster. It supports the importance of the ratio between anode and cathode area. The impact from the crack width seem to rule the time to initiation of corrosion, but after initiation the corrosion develops at the same rate. There is a clear correspondence between ongoing fibre corrosion and loss of residual strength especially on load-bearing capacity at large deformations (ultimate limit state).

The chloride contents in the samples along Rv40 and in the Eugenia tunnel are high after exposure which also accelerate the initiated corrosion heavily. In the tunnel there is an accumulation of chlorides since the samples have been sheltered to precipitation.

To conclude it can be stated that steel fibre corrosion in cracked concrete exposed to an environment with chlorides from de-icing salts must be expected to occur for the most commonly used fibre types. It is not realistic to expect a service-life of 100 years with remained load-bearing capacity in the tested chloride exposed environments.

REFERENCES

[1] Nordström, E.: “Durability of Sprayed Concrete – Steel Fibre Corrosion in Cracks”, Doctoral Thesis, 2005:02, Luleå University of Technology, 151 pp, (2005)

[2] Nordström, E.: “Experiences from 10-year field exposure of cracked steel fibre reinforced shotcrete”, Proceedings, Spritzbeton-Tagung, Alpbach, Austria, 17 pp., (2009)

[3] Nordström, E.: “Utvärdering efter 17 års fältexponering av sprucken stålfiberarmerad sprutbetong” (In Swedish), BeFo report no. 153, Sweden, 34 pp., (2016)

Extending service life by coupling the limit states of corrosion initiation and corrosion induced cracking

Edgar Bohner
M.Sc, Dr. -Ing.
VTT Technical Research Institute of Finland Ltd.
Kemistintie 3, P.O. Box 1000
FIN-02044, Espoo, Finland
edgar.bohner@vtt.fi

Miguel Ferreira
M.Sc, Ph.D.
VTT Technical Research Institute of Finland Ltd.
Kemistintie 3, P.O. Box 1000
FIN-02044, Espoo, Finland
miguel.ferreira@vtt.fi

ABSTRACT
The service life design of reinforced concrete structures requires models capable of reliably describing both the mechanisms of damage and its progression over time. For concrete exposed to chlorides, service life design typically disregards the onset of damage, i.e. the progress of corrosion of the reinforcing steel. Common service life design practice typically considers the end of the initiation phase of the degradation process as the design limit state. A method is proposed where a model for estimating the time to corrosion initiation is coupled with a model for estimating the time to corrosion induced cracking into a single limit state determination. An example is provided of a structural element that has been designed for the serviceability limit state of corrosion induced concrete cover cracking. The results show that the corrosion rate is a major factor for the coupled service life determination. Where fast corrosion is expected, service life extension is insignificant, and where slow corrosion rates are expected, service life extension can be significant.

Key words: Service life, limit state, design, modelling, deterioration, concrete cover, chloride ingress, corrosion, cracking, serviceability.

1. INTRODUCTION

A method that combines the probabilistic determination of two limit states (corrosion initiation and corrosion induced cracking) in a single calculation has been developed [1, 2]. If durability design is performed considering the limit state of corrosion induce cracking, then this method eliminates the need for an intermediate limit state, that of corrosion initiation. By combining a model for corrosion initiation with a model for corrosion induced cracking, the coupled service life covers the period from $t = 0$ to the appearance of the first reinforcement corrosion induced crack with a minimum width of 0.05 mm on the surface of the concrete.
Assuming that corrosion is initiated at some time τ, for cracking to take place at time t, the

corrosion process has a duration of $t-\tau$. Consequently, the combined probability distribution of the time of cracking is

$$f_{i,p}(t) = \int_{-\infty}^{\infty} f_p(t-\tau \mid T_i = \tau)\ f_i(\tau)\, d\tau \quad (1)$$

where $f_{i,p}$ = probability of failure; $f_i(t)$ = probability distribution function of the initiation model; and $f_p(t)$ = probability distribution function of the propagation model.

The start of corrosion propagation depends on the initiation of corrosion process, however, the mechanisms that describe each of these processes are independent of each other. Therefore the modelling and computation of the distribution in Eq. (1) can be simplified by replacing the conditional probability distribution function with corresponding marginal probability distribution,

$$f_{i,p}(t) \approx \int_{-\infty}^{\infty} f_p(t-\tau)\ f_i(\tau)\, d\tau \quad (2)$$

The model assumes chloride ingress starts at the time of construction ($t = 0$), and that the corrosion process starts when chloride has reached a critical threshold value at the depth of the reinforcement. Consequently,

$$f_p(t) = f_i(t) = 0 \quad \forall \ t < 0 \quad (3)$$

allowing the integration interval to be shortened. For $t \geq 0$

$$f_{i,p}(t) \approx \int_{0}^{t} f_p(t-\tau)\ f_i(\tau)\, d\tau \quad (4)$$

This method, by coupling the corrosion initiation with the corrosion propagation process, eliminates the need to define the limit state criteria for the initiation of corrosion process. There is no consensus yet as to what constitutes the correct criteria for assessing the corrosion initiation limit state [3]. Furthermore, the event that defines the corrosion initiation limit state cannot be observe visually. In contrast, the coupled method is defined by a limit state event that can be observed on the structure, i.e., the appearance of the first corrosion induced crack.

2. SERVICE LIFE CALCULATION

The implementation of this method requires models for both corrosion initiation and for corrosion induced cracking. The approach is based on the coupling of the probability distribution function outcome for each model, so is not model specific. For the calculations presented here, the following models have been used for corrosion initiation and corrosion propagation [1, 2].

2.1 Brief example description

To demonstrate the method, a hypothetical semi-infinite reinforced concrete wall located in a XS3 environment (tidal/splash zone) is considered. For this scenario, a 1-D analysis is conducted considering diffusion as the main form of chloride transport in the concrete (convection zone not considered in this study).

Service life calculations were performed considering two distinct concrete qualities: a CEM I 42.5 N with w/b ratio 0.50, and a CEM III/A 42.5 R with w/b ratio 0.55. Both concretes have similar mechanical performance, but differ significantly from a durability perspective considering chloride ingress, where CEM III outperforms CEM I. Details for the model

parameters, distribution types and values are given in [1]. For the corrosion propagation model, two corrosion rates were chosen to simulate varying speeds of corrosion: 5.0 μA/cm^2 and 0.5 μA/cm^2. Corrosion rate is defined by a lognormal distribution (CoV = 0.3) with average values of 0.0525 mm/year and 0.00525 mm/year, respectively.

2.2 Results

The calculation of the limit states for both initiation and propagation models separately was performed with a direct Monte Carlo simulation based on 10^4 determinations for each time step. The probability density function in Eq. 4 was computed with trapezoidal numerical quadrature, as described by [4]. For the purpose of demonstrating this method, the coupled limit state criteria is assumed to be 10 %.

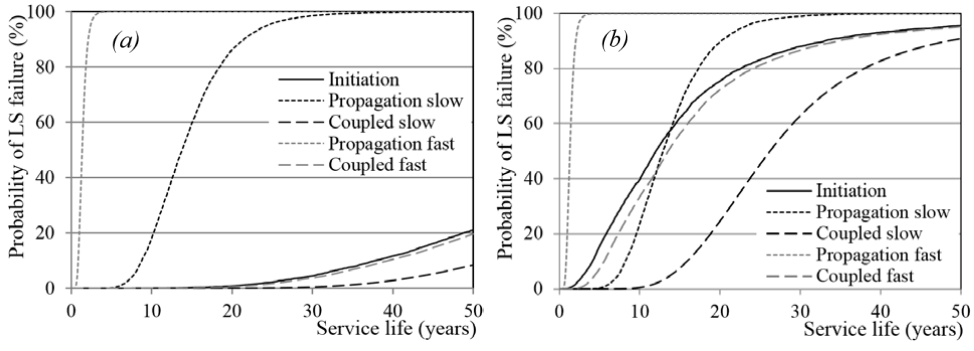

Figure 1 – Probability of limit state failure for corrosion initiation, corrosion propagation, and coupled limit state for both (a) CEM III concrete and (b) CEM I concrete, and for varying corrosion rates: 0.0525 mm/year ("fast") and 0.00525 mm/year ("slow").

The service life obtained by combining the two individual service life calculations depends on both the quality of concrete and the corrosion rate. However, it is clear that the quality of concrete, mostly determining the time to corrosion initiation, dominates the service life calculation as it is the precursor for the corrosion propagation phase. The results show that the corrosion rate has a significant influence in the extension of the service life. If the corrosion rate is "fast" then no significant increase in service life is obtained (< 2 years for both concretes). If the corrosion rate is "slow", a significant increase in service life is obtained (> 10 years for both concrete).

Table 2 – Time (years) until the criteria of 10% has been exceeded for the initiation, propagation and coupled limit state calculations.

CEM I	"Fast"	"Slow"	CEM III	"Fast"	"Slow"
Initiation	4.1	4.1	Initiation	37.8	37.8
Propagation	0.8	8.2	Propagation	0.9	8.8
Coupled	5.6	15.9	Coupled	39.5	52.1
SL extension	1.5	11.8	SL extension	1.7	14.3

Cairns & Law [5] have suggested that the limit state for corrosion induced cracking should be considered in an identical manner as the corrosion initiation limit state because the appearance

of the first crack does not affect the mechanical performance of the reinforced concrete structures.

3 CONCLUSIONS

A probabilistic method that couples the calculation of two independent limit states for concrete deterioration: chloride induced corrosion initiation and corrosion induced cover cracking of concrete is briefly described. By combining these two limit states, the outcome of the service life calculation is the probability of time to corrosion induced cracking, at any time starting after construction. The method is demonstrated with two concrete qualities (CEM I and CEM III) and two corrosion rates (5.0 $\mu A/cm^2$ and 0.5 $\mu A/cm^2$).

An immediate advantage of the coupling of both processes is that the limit state event that defines the coupled method can actually be observed on the structure, i.e., the appearance of the first corrosion induced crack. This eliminates the needs for the definition of the corrosion initiation limit state criteria, which cannot be observed in practice.

The results show that the corrosion rate is a major factor to consider when determining the service life of a reinforced concrete structure. In situations where fast corrosion can be expected, due to either poor concrete quality and/or an aggressive environment, the propagation model, when coupled to the initiation model, does not extend the service life calculation significantly (< 2 years for the cases studied). However, when slower corrosion rates are expected, this can affect positively the service life calculation by extending significantly the design service life (up to almost 15 years for the given examples).

The crux of this approach, which is not intrinsic to this method, resides in the definition of the limit state requirement for the coupled method (reliability index or probability of limit state failure). There is currently insufficient information to understand the consequences of certain values, and while many values are being put forward based on those used in structural design, they do not necessarily represent adequately the complexity of the deterioration mechanism and the economic consequences of limit state failure.

This study shows the benefit of using a coupled limit state analysis until the time to first corrosion induced crack to appear. The joint consideration of corrosion initiation and propagation describes the relationship between the damage mechanisms more realistically, enabling potential extension of the service life of the structures. Increased accuracy in assessment of the performance of the reinforced concrete structures enables optimised resource management.

REFERENCES

[1] Ferreira, M., Bohner, E., Saarela, O., (2016) *Designing concrete durability by coupling limit states of corrosion initiation and corrosion induced cracking of concrete cover*. Nordic Concrete Research Journal. NCR 54 - 1/2016, pp. 7-20.

[2] Bohner, E., Ferreira, M., Saarela, O., (2016) *Parametric study of coupled models for corrosion initiation of reinforcement and induced cracking of concrete cover*. Fib Symposium 2016, South Africa, Cape Town. 8p.

[3] Gulikers, J. (2006) *Critical issues in the interpretation of results of probabilistic service life calculations*. in Int. RILEM Workshop on Integral Service Life Modelling of Concrete Structures. Guimarães, Portugal, ISBN 972-99179-2-2. 195-204.

[4] Stoer, J., Bulirsch, R. (1980) *Introduction to numerical analysis*. Springer-Verlag: Berlin.

[5] Cairns, J., Law, D., (2003) *Prediction of the ultimate limit state of degradation of concrete structures*. ILCDES 2003: Integrated Lifetime Engineering of Buildings and Civil Infrastructures. Rotterdam. 6.

µ-XRF – Characterisation of chloride ingress and self-healing in cracked concrete

Tobias Danner*
MSc, PhD, Researcher
tobias.a.danner@ntnu.no

Klaartje De Weerdt*
MSc, PhD, Associate professor
klaartje.d.weerdt@ntnu.no

Mette Rica Geiker*
MSc, PhD, Professor
mette.geiker@ntnu.no

*
Norwegian University of Science and Technology
Department of Structural Engineering
Richard Birkelandsvei 1a, NO-7491 Trondheim

ABSTRACT
In this paper we illustrate the applicability of µ-XRF for investigations of chloride ingress and self-healing in cracked concrete. A cracked and an uncracked concrete core exposed to seawater for more than 30 years were investigated with µ-XRF. The cracked sample had higher chloride ingress in the outer part of the concrete core (first 20 mm). Parts of the investigated crack were self-healed with calcium and magnesium rich phases. It was concluded that µ-XRF is a powerful tool for fast and detailed characterization of elemental distribution; e.g. chloride ingress, as it is able to detect spatial irregularities caused by for example cracks.

Key words: Cracking, Chlorides

1 INTRODUCTION

As part of the Norwegian Public Road Authorities (NPRA) Ferry-free coastal road E39 project, NTNU is collecting long term data from field exposed reinforced concrete structures on chloride ingress and the extent of corrosion in the vicinity of cracks.

There is agreement in literature that cracks in concrete increase the ingress of harmful species like chloride ions [1]. However, it is also expected that in the long term effects like self-healing of cracks may reduce the later chloride ingress [1, 2]. In case of a self-healed crack the chloride ingress depends on the resistance to ingress of the "healing" phase. The most commonly used technique to analyse chloride ingress in concrete is profile grinding of extracted cores and subsequent chemical analysis for chlorides [3]. However, this method is destructive and time consuming. Furthermore, the collected powder is homogenized over the entire area; thus, the potential impact of cracks on ingress will be unclear. 2D characterization of chloride ingress might be obtained by spraying the surface with $AgNO_3$, which reacts with available chlorides. The method was for example used by Michel et al. (2013) to illustrate the ingress through primary cracks and debonding between concrete and reinforcement [4]. The disadvantage of the method is that only the depth of penetration of a given threshold is determined. SEM and µ-XRF (µ-X-ray fluorescence) and other chemical imaging techniques,

on the other hand, can provide equivalent or better information to profile grinding and in 2D [5]. Similar to bulk XRF, µ-XRF uses X-ray excitation to induce characteristic X-ray fluorescence emission from the sample for elemental analysis. Compared to other chemical imaging techniques, µ-XRF has two major advantages. µ-XRF is less sensitive to surface roughness and there is no or only little sample preparation required [5]. Furthermore, big samples up to 20 x 15 cm with a weight up to 5 kg can be measured. Thus, µ-XRF can fast deliver results on large concrete samples. Besides chloride mapping other elements can be investigated and local abnormalities like cracks or other forms of chemical attack can be detected additionally [5].

The objective of this study is to illustrate the applicability of µ-XRF for characterization of chloride ingress and self-healing of cracks in concrete.

2 MATERIALS AND METHODS

A cracked and an uncracked concrete core exposed to seawater for more than 30 years were investigated. The cores had a length of 200 mm and a diameter of 100 mm. The cracks in the cracked concrete were measured with a crack-width ruler. The crack width varied unsystematically between 0.3-0.7 mm. The crack was perpendicular to the exposed surface and oriented transverse to the main reinforcement and parallel to the stirrups. The cores were cut perpendicularly to the surface with a water-cooled concrete saw in two halves. One half of each core was sprayed with a 0.1 M $AgNO_3$ solution and the chloride ingress was measured with a slide gauge according to [6].

The other halves were without further preparation investigated with a M4 Tornado µ-XRF apparatus from Bruker. The instrument uses a silicon drift detector energy dispersive spectrometer (SDD-EDS). The µ-XRF is equipped with a silver X-ray tube and polycapillary lenses focusing the X-ray beam to a spot size of 25µm. For point analysis, a current of 200 µA and a voltage of 50 kV were used. For line scans and elemental mapping the current was increased to 600 µA. The chamber pressure was 20 mbar at all times. The elemental mapping area was 150 x 50 mm.

Preliminary results on the chloride ingress in a cracked (CC) and an uncracked concrete (UC) core and self-healing of cracks are presented.

3 RESULTS AND DISCUSSION

Figure 1 shows an elemental map of the cracked concrete core including Cl, Ca, Si, Al, Fe, Na, K, Mg and S. No sample preparation was required and the data acquisition took 2.5 h.

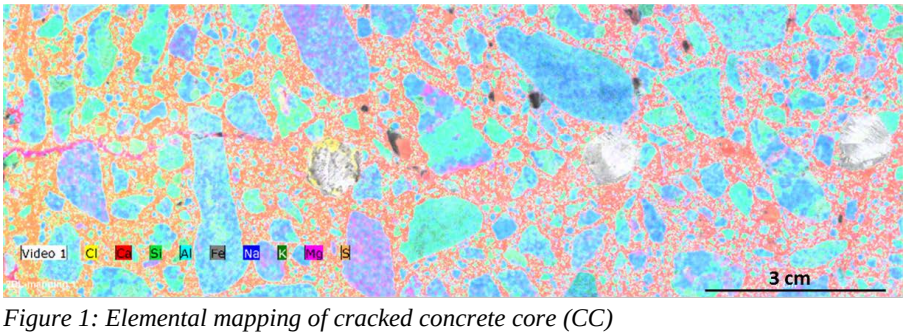

Figure 1: Elemental mapping of cracked concrete core (CC)

Chloride maps of the cracked and the uncracked concrete cores are shown in Figure 2. In the maps, the chloride ingress depth measured with $AgNO_3$ is indicated with the light grey area.

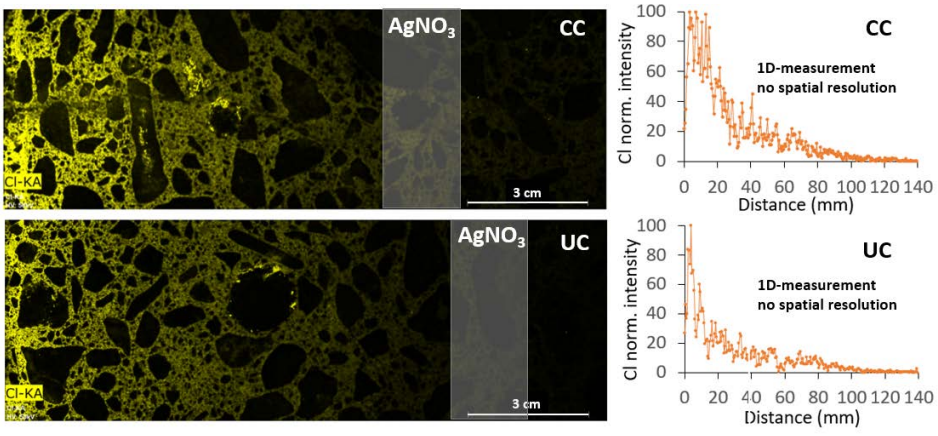

Figure 2: Qualitative 2D-chloride map of cracked ('CC', above) and uncracked concrete cores ('UC', below), as well as normalized intensity of chloride line scans from the surface to the bulk of the cores (average of six line scans)

Next to the chloride maps in Figure 2, the measured normalized intensity of chloride as a function of the depth from the surface is shown. The results show an average of six line scans, each with 250 measuring points.

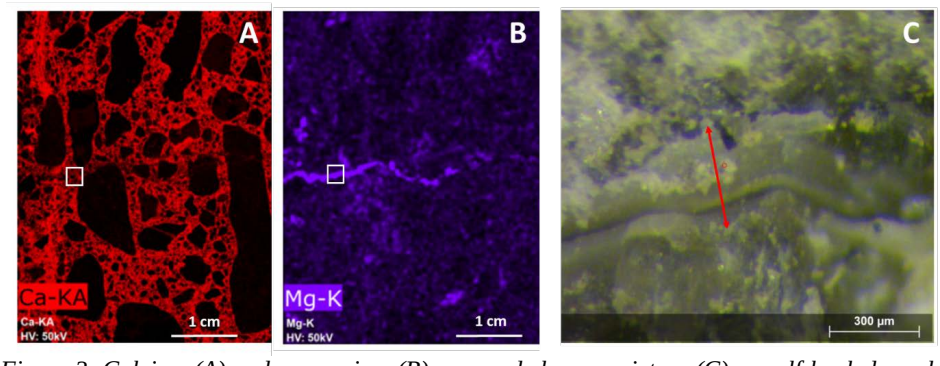

Figure 3: Calcium (A) and magnesium (B) map and close up picture (C) on self-healed crack in cracked core (red line indicating original crack width)

µ-XRF showed that the cracked core has higher chloride levels in the outer 20 mm. However, the total depth of chloride penetration is comparable in the cracked and uncracked concrete. By spraying with silver nitrate the detected chloride penetration was slightly lower in the cracked concrete compared to the uncracked concrete (Figure 2). The reason for this is at present unknown.

Figure 3 shows calcium and magnesium maps in addition to a close up picture of a self-healed crack in the cracked core (CC). It appears that precipitated solids almost close the crack. The red arrow in Figure 3C is marking the original crack width of about 0.4 mm in the

shown area. Similar areas were found all over the sample where the crack was almost completely healed. Point analysis was performed on the phases precipitated in the crack. The results showed that the phases are rich in calcium and magnesium with a ratio of about 1/1, indicating the potential presence of e.g. dolomite.

In other areas the crack appeared open or was filled with debris potentially from the cutting of the cores. Self-healing of the crack can explain why the total depth of chloride penetration was comparable in the cracked and uncracked cores, even with a crack width of up to 0.7 mm in some parts.

4 PERSPECTIVES

µ-XRF is shown to be a powerful tool for fast elemental analysis (e.g. chloride ingress) of large concrete samples with little effort. With a spatial resolution of 25 µm it is in addition feasible for detailed analysis of areas of specific interest. In this investigation self-healing of a crack was characterized.

ACKNOWLEDGEMENT

The NTNU Dean's fund for scientific equipment is acknowledged for subsidizing the purchase of the µ-XRF. This research is part of the Norwegian Public Roads Administration (NPRA) Ferry-free coastal route E39 project. DNV GL is acknowledged for providing the concrete columns.

REFERENCES

1. Jacobsen, S., J. Marchand, and L. Boisvert, *Effect of cracking and healing on chloride transport in OPC concrete.* Cement and Concrete Research, 1996. **26**(6): p. 869-881.
2. Savija, B. and E. Schlangen, *Autogenous healing and chloride ingress in cracked concrete.* Heron, 2016. **61**(1): p. 15-32.
3. *ASTM C1152 - Standard Test Method for Acid-Soluble Chloride in Mortar and Concrete*. 2012.
4. Michel, A., et al., *Experimental investigation of the relation between damage at the concrete-steel interface and initiation of reinforcement corrosion in plain and fibre reinforced concrete.* Cement and Concrete Research, 2013.
5. Khanzadeh Moradllo, M., et al., *Using micro X-ray fluorescence to image chloride profiles in concrete.* Cement and Concrete Research, 2017. **92**: p. 128-141.
6. NPRA, *436 Kloridinntregning i betong ved fargemetode*, in *R210 Laboratorieundersøkelser*. 2015, National Public Roads Administration. p. 349-350.

Corrosion-induced cracking and bond behaviour of corroding reinforcement bars in SFRC

Carlos G. Berrocal, PhD student, Chalmers University of Technology & Thomas Concrete Group AB, Gothenburg, Sweden.
carlos.gil@chalmers.se

Ignasi Fernandez, Senior lecturer, Chalmers University of Technology, Gothenburg, Sweden.
ignasi.fernandez@chalmers.se

Ingemar Löfgren, PhD, Thomas Concrete Group AB, 402 26 Gothenburg, Sweden.
ingemar.lofgren@c-lab.se

Karin Lundgren, PhD Professor, Chalmers University of Technology, Gothenburg, Sweden.
Karin.lundgren@chalmers.se

ABSTRACT

In this study, an experimental programme has been carried out to investigate the influence of fibres on the onset of corrosion-induced splitting cracks. Cylindrical lollipop specimens with a centrally positioned Ø16 mm bar and varying cover depths from 40 to 64 mm were subjected to accelerated corrosion. A constant current of 100 µA/cm^2 was impressed through the specimens and the electrical resistance between each rebar and an external copper mesh acting as cathode was monitored. The fibres, due to their confining effect, contributed to delay crack initiation, improve the post-peak bond behaviour and retain the initial splitting strength for corrosion levels of up to 8%.

Key words: Chlorides, Corrosion, Cracking, Fibres, Reinforcement.

1. INTRODUCTION

The present study aimed at investigating two distinct phenomena which have been seldom addressed in the past, namely: (1) the influence of steel fibres at low dosages on the onset of splitting cracks induced by corroding conventional reinforcement; and (2) the bond behaviour of corroded reinforcement bars embedded in steel fibre reinforced concrete (SFRC). These aspects were addressed experimentally and the results include the corrosion level associated to crack initiation, crack width measurements of corrosion-induced cracks, the evolution of the bond strength with increasing corrosion and a comparison of the anchorage capacity based on the local bond-slip relationship obtained. For a more detailed description of the results see [1].

2. EXPERIMENTAL PROGRAMME

The experimental programme involved 42 specimens and to assess the influence of fibres on the bond capacity of corroded reinforcement bars pull-out tests were performed at three different corrosion stages. Accordingly, the specimens were divided into three groups: group I, uncorroded specimens used as reference samples; group II, specimens corroded up to the onset of corrosion-induced cracking; and group III, specimens corroded beyond the onset of splitting cracks. Furthermore, two different cover to bar diameter (Ø 16 mm) ratios, *c*/Ø, were

investigated for the bond-behaviour and a third one was included for the crack initiation stage. Table 1 summarizes the details of the experimental programme.

Table 1. Experimental programme.

	Corrosion stages and concrete type					
	Group I Uncorroded - Reference		Group II Crack onset		Group III High corrosion	
c/Ø ratio	PC	FRC	PC	FRC	PC	FRC
2.5	x	x	x	x	x	x
3.25	-	-	x	x	-	-
4.0	x	x	x	x	x	x

Note: Three specimens were cast for each combination of *c*/Ø ratio and corrosion stage investigated.

A self-compacting concrete mix with a water to cement ratio (*w*/*c*) of 0.47 was prepared to cast all the specimens using individual moulds. The same mix composition was used to prepare both the plain and the steel fibre reinforced concrete, except for minor variations in the aggregate content to incorporate the fibres. End-hooked Dramix steel fibres, 35 mm long with diameter 0.55 mm, were used as fibre reinforcement at a dosage of 40 kg/m^3. Sodium chloride was incorporated into the mix at 4% by weight of cement with the intention of preventing the formation of the passive layer on the steel bar. The accelerated corrosion and the pull-out setup is presented in Figure 1.

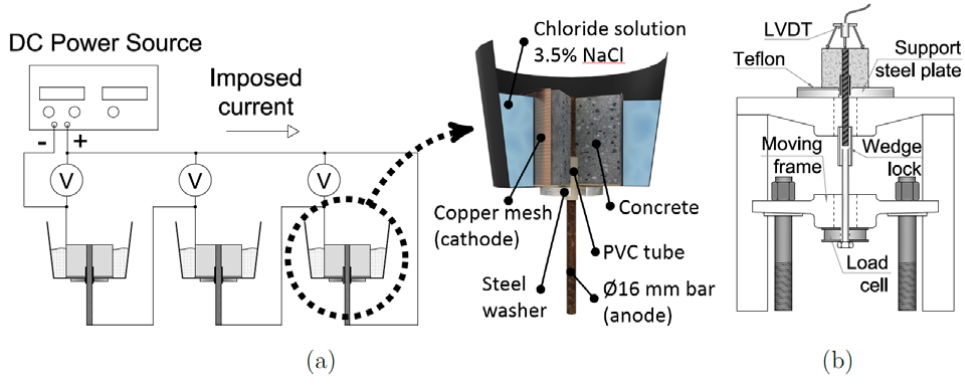

Figure 1. Accelerated corrosion setup (a) and the pull-out test (b) (bonded length 70 mm).

3. RESULTS AND DISCUSSION

The relation between corrosion level, defined as the steel loss assumed to be concentrated and uniformly distributed along bonded length of the bar, and crack initiation is presented in Fig. 2. The results clearly shows that, from the parameters investigated in this study, the *c*/Ø played the most important role in delaying the initiation of corrosion-induced cracks, although its effect was more pronounced in PC specimens. Increasing the *c*/Ø from 2.5 to 4.0, delayed crack initiation by a factor of 2 and 1.5 for PC and FRC specimens in Group II, respectively, whereas it delayed crack initiation by a factor of 4 and 1.75 for PC and FRC specimens in Group III, respectively. Adding fibre reinforcement had likewise a positive effect in delaying crack

initiation, although to a lesser degree compared to the $c/\emptyset$, which was particularly noticeable in small $c/\emptyset$ test specimens.

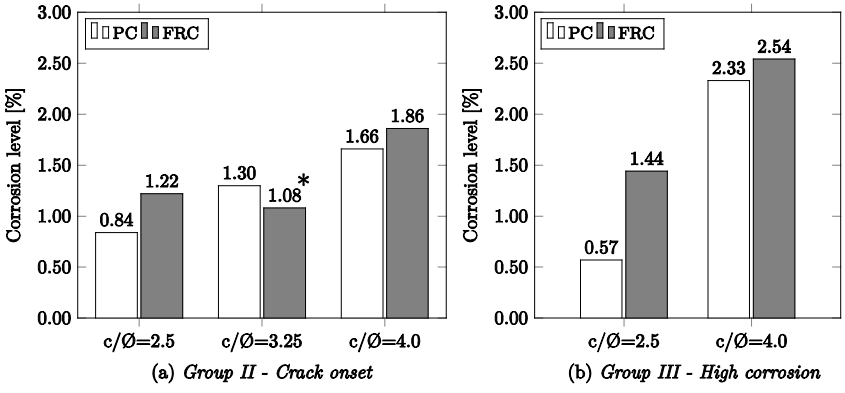

*Figure 2. Average corrosion levels at crack initiation. *FRC specimens with c/Ø=3.25 in Group II deviated from the general trend followed by the rest of specimens and were considered outliers.*

In order to compare the pull-out test results of the PC and FRC specimens for the different covers and corrosion stages in detail, the splitting strength from each experimental curve is presented in Figure 3(a) as a function of the corrosion level. As expected, for the reference group, there was not a significant difference between PC and FRC in terms of splitting strength since the fibres did not prevent cracking, whereas a small increase, attributable to the cover size, was apparent. Upon corrosion-induced cracking, PC specimens suffered a moderate reduction of the splitting strength whereas it slightly increased for FRC, an effect that may be attributed to a higher normal stress at the interface due to corrosion. Finally, at higher corrosion levels the remaining splitting strength of PC specimens was only a small fraction of the initial, with no apparent influence of the cover depth. Highly corroded FRC specimens, on the other hand, exhibited a nearly identical splitting strength as uncorroded ones.

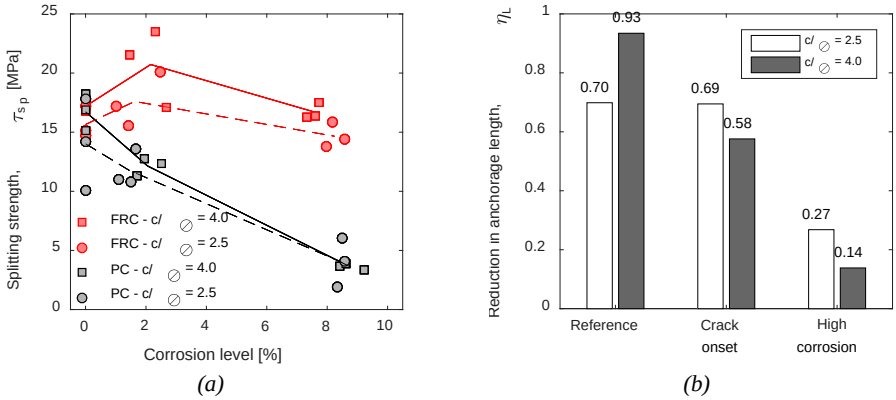

Figure 3. (a) Splitting strength determined experimentally as a function of the corrosion level at structural testing for PC and FRC (lines show the average behaviour). (b) Reduction in the needed bar length to anchor the yield strength of a Ø16 mm rebar with yield stress 550 MPa in FRC compared to PC, obtained using 1D numerical analysis and the experimental bond-slip as input.

Figure 3(b) shows the reduction of anchorage length in FRC compared to PC to fully anchor the yield strength of the rebar, expressed as the fraction of length needed. The addition of fibres resulted in an anchorage length reduction of 30% at an uncorroded stage, whereas that effect was not as evident for large specimens due to the higher confinement provided by the concrete cover. These results show that as the cover increases and approaches "well confined" conditions ($c/Ø = 5$ according to Model Code 2010 [2]), the beneficial effect of the fibres on the anchorage length decreases, which is in line with results reporting that low fibre contents will not significantly influence the behaviour of RC elements exhibiting pull-out failure.

4. CONCLUSIONS

This paper briefly reports experimental results regarding the corrosion level associated to the initiation of splitting cracks in PC and FRC, as well as results of pull-out tests with short-embedment length carried out for both PC and FRC at various corrosion stages. Based on the results of the study, the following conclusion may be drawn:

(1) The use of steel fibres at a 0.5% vol. dosage provided an additional source of passive confinement that delayed corrosion-induced cracking. This effect was more noticeable in specimens with a smaller c/Ø, whereas it became less apparent for larger $c/Ø$ in which the cover already provided a significant confinement to the rebar.

(2) As expected, for uncorroded specimens, the results from the pull-out tests showed no significant difference between PC and FRC specimens regarding the splitting strength. For increasing corrosion levels, however, the splitting strength of PC specimens exhibited a clear degradation, particularly for specimens with a larger cover. Conversely, FRC specimens retained their initial splitting strength at 8% corrosion and even showed a slight increase at intermediate corrosion levels.

(3) The pull-out tests revealed a clear contribution of the fibres on the post-peak capacity regardless of the size and corrosion level. Based on the 1D analyses, the anchorage length in FRC specimens subjected to 8% corrosion was only increased by 10% compared to uncorroded reference specimens, unlike for PC specimens in which the anchorage length at the same corrosion level increased by a factor ranging from three to seven.

In addition to what has been presented in this paper, crack width measurements revealed that cracks in FRC were around half as wide at corrosion levels approaching 8%. Moreover, fibre reinforcement proved to be an effective means of preventing spalling of the concrete cover, understood as both its physical detachment and the loss of its mechanical contribution to the structure.

REFERENCES

[1] Berrocal, C. G., Fernandez, I., Lundgren, K., Löfgren, I.: Corrosion-induced cracking and bond behaviour of corroded reinforcement bars in SFRC. Composites Part B: Engineering, Volume 113, 15 March 2017, pp. 123–137.

[2] Model Code 2010, *fib* model Code for concrete structures. Weinheim, Germany: Wiley-VCH Verlag GmbH & Co. KGaA; 2010.

Corrosion probability and service life in reinforced concrete facades in Nordic climate

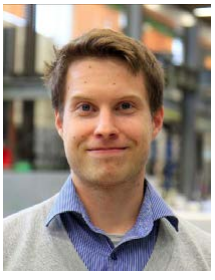

Arto Köliö
D.Sc., Postdoctoral researcher
Tampere University of Technology
Korkeakoulunkatu 5, FI-33720 Tampere, Finland
e-mail: arto.kolio@tut.fi

Jukka Lahdensivu
Adjunct professor, D.Sc.
Tampere University of Technology
Korkeakoulunkatu 5, FI-33720 Tampere, Finland
e-mail: jukka.lahdensivu@tut.fi

Matti Pentti
Professor, D.Sc.
Tampere University of Technology
Korkeakoulunkatu 5, FI-33720 Tampere, Finland
E-mail: matti.pentti@tut.fi

ABSTRACT
A vast number of concrete buildings utilizing newly developed prefabrication techniques were built in Finland from 1960 to1979. Since then, the durability properties of this concrete building stock have been found to be poor. Corrosion of reinforcement in these structures is not easily predicted because a methodology for this does not exist. We studied the relevance of the active corrosion phase in the concrete service life by advanced statistical and experimental studies. It was confirmed that the active corrosion phase can provide a considerable extension to the residual service life of these structures in Nordic climate especially in certain conditions.

Key words: Concrete, Carbonation, Corrosion, Facades, Service life, Modelling.

1. INTRODUCTION

The majority of the existing concrete facades in Finland have been built in time when service life design practice was not yet established. A widely accepted description of the corrosion process of steel in concrete withholds the phases of initiation and propagation [1]. The reinforcement service life is in Finnish practice defined as only corrosion initiation. Meaning that the target service life should be achieved by carbonation resistance. In already aged existing

buildings, the initiation phase has in many cases already passed. This forms two problems: (i) the residual service life is, by the definition, zero even though no damage at all has happened, (ii) there are no methods available to evaluate the residual service life. This study focuses on the problematic behind service life design and maintenance of existing concrete facades in Finland.
The research objective was to study how significant the active corrosion phase is in these structures' service life. Statistical studies, complemented with laboratory studies, on the corrosion probability and its effect on reinforced concrete service life are presented in this paper.

2. RESEARCH MATERIAL AND METHODS

Studies on the rate and extent of reinforcement corrosion in concrete facade panels were conducted combining the analysis of specific experimental research material gathered from 12 visually corrosion damaged concrete buildings to statistical data gathered from standardized condition investigation reports [2]. The realized service life of concrete facades in regard of visual damage caused by reinforcement corrosion was studied statistically from a database of 947 buildings [3] based on the age of the concrete facades and visual damage ratings/classification (no visual damage, incipient damage, wide spread damage).

Corrosion rate was studied as a combined effect of weather parameters on already carbonated concrete structures exposed to natural outdoor environment in both inland and coastal area locations [4]. Long term corrosion rate measurement data [5] was combined with weather data from the location of the measurements from the same time period. A linear regression model was formed on the basis of linear regressions between the individual weather parameters and the corrosion rate. From a relatively large number of analyses (525 analyses with different combinations of weather parameters, seasons, etc.) the best performing combinations were judged by the coefficient of de-termination (R^2) of the model.

3. RESULTS AND DISCUSSION

3.1. Statistical analysis on service life

Service life monte carlo -analysis for varying facade structures is presented for initiation period and for propagation period (Fig. 1). The initiation period is, by 10 % fractile, 24 years for brushed and painted concrete, 21 years for exposed aggregate concrete, 11 years for the balcony side panels and 10 years for the balcony slab soffit surface. The target service life is therefore in these existing structures not achieved by the initiation phase alone. However, if the reinforcement is placed according to requirements with sufficient concrete cover, the target service life of 50 years can be easily achieved by initiation alone.

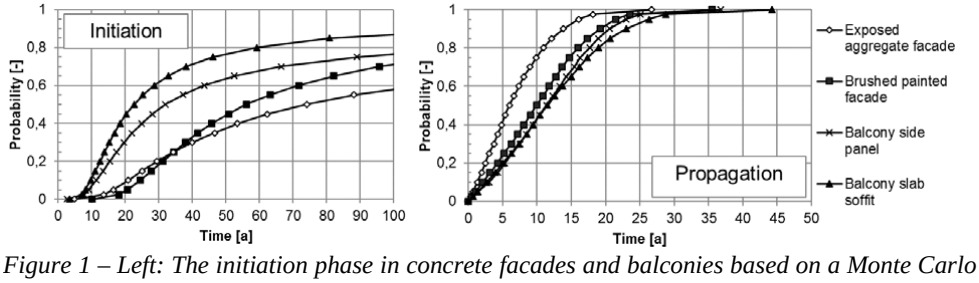

Figure 1 – Left: The initiation phase in concrete facades and balconies based on a Monte Carlo simulation on statistical condition assessment data from buildings constructed in 1965–1990. Right: The propagation phase in concrete facades and balconies based on a Monte Carlo simulation.

With the same 10 % fractile, the propagation time can be expected to be very short from 1.5 to 3 years (Fig. 1). This safety level relates to the most critical conditions for corrosion of reinforcement with extremely small cover depth or in very capillary concrete. However, this safety level may be too strict compared to empirical knowledge. As the effects of corrosion in this context are mainly visual defects, a safety level of 50% could be applied. In these cases the active corrosion period would be 6–12 years depending on the surface type. Even though corrosion is propagated quite fast in the both facade surfaces their initiation phase is quite long. Vice versa, balcony slab soffits and balcony side panels are shown to have a significantly shorter initiation phase but their propagation phase tends to be longer. It is shown by this statistical comparison that favourable parameters and conditions to initiation and propagation phases tend to at least to some extent be opposite to each other. In service life design the initiation phase is still the primary part in ensuring sufficient service life.

3.2 The corrosion rate in Finnish climate

Separate regression models for corrosion rate in regard of weather were produced from the time series data for the facades and balconies in both the inland and the coastal areas. A fairly good fit (R^2 of 0.49–0.53) was found in the cross-checking (using the coastal area model inland and vice versa). Finally, a composite model was produced with inland and coastal data (R^2 of 0.71-0.55). The generated model intends that average corrosion rate levels in carbonated concrete caused by the prevailing weather are 0.7–1.4 µA/cm^2 in inland and 1.0–1.8 µA/cm^2 in the coastal area (Fig. 2). An average critical corrosion penetration limit of 67.5 µm [6] was utilized in the below figures (dashed line).

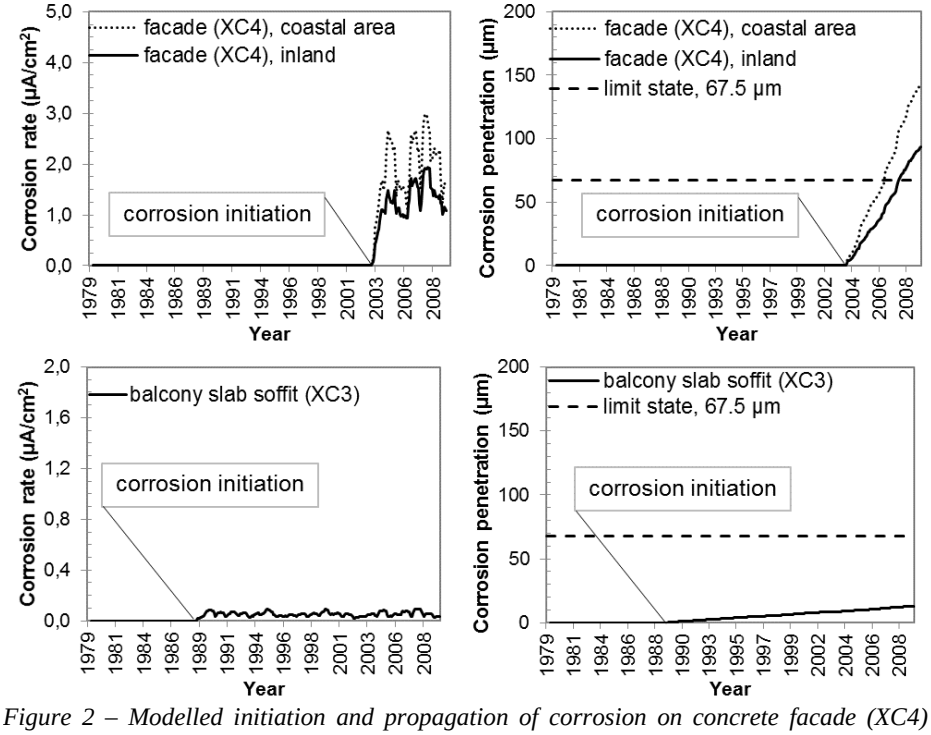

Figure 2 – Modelled initiation and propagation of corrosion on concrete facade (XC4) and balcony slab soffit (XC3) given as the corrosion rate (Left) and corrosion penetration (Right).

Critical corrosion penetration is presented as a dashed horizontal line. NOTE! The different scale on the corrosion rate (y-axis).

4. CONCLUSIONS

The research project confirmed that the active corrosion phase can provide a considerable extension to the residual service life of concrete facade panels in a Nordic climate. Our statistical analyses show that the length of this period can be from a few to up to 30 years. A more in-depth analysis of the case-study buildings, however, showed that the service-life extension for XC4 exposure conditions is, in practice, likely to be limited to well below ten years. In structures which, for a variety of reasons, are more sheltered from wind-driven rain, the extension in service life can be considerably higher. This is especially true for sheltered structural surfaces, such as the soffit surfaces of the balcony slabs. It has to be noted that the limit is based on the occurrence of visible corrosion damage on the structure surfaces. Even this is therefore not the ultimate end of service life for these structures.

REFERENCES

[1] Tuutti K. 1982. Corrosion of steel in concrete. Stockholm. Swedish Cement and Concrete Research Institute. CBI Research 4:82. 304 p.

[2] Lahdensivu J, Varjonen S, Pakkala T, Köliö A. 2013. Systematic condition assessment of concrete facades and balconies exposed to outdoor climate. Int. J. of Sustainable Building Technology and Urban Development, 4:3(2013). Pp. 199-209.

[3] Köliö A, Pakkala TA, Annila PJ, Lahdensivu J, Pentti M. 2014. Possibilities to validate design models for corrosion in carbonated concrete using condition assessment data. Engineering Structures, 75(2014). Pp. 539-549.

[4] Köliö A, Hohti H, Pakkala T, Laukkarinen A, Lahdensivu J, Mattila J, Pentti M. 2016. The corrosion rate in reinforced concrete facades exposed to outdoor environment. Materials and Structures

[5] Mattila J, Pentti M. 2008. 2008. Residual service-life of concrete façade structures with reinforcement in carbonated concrete in Nordic climate. Tailor Made Concrete Structures, Taylor & Francis Group, London. Pp. 75-79.

[6] Köliö A, Honkanen M, Lahdensivu J, Vippola M, Pentti M. 2015. Corrosion products of carbonation induced corrosion in existing reinforced concrete facades. Cement and Concrete Research, 78(2015). Pp. 200-207.

Durability assessment and service life design for reinforced concrete exposed to chloride ingress – an easy to use design diagram

Claus Vestergaard Nielsen
M.Sc., Ph.D.
Senior Chief Specialist
Rambøll Denmark A/S
Prinsensgade 11, DK-9000 Aalborg
e-mail: cvn@ramboll.dk

ABSTRACT
It is anticipated that design for service life and assessment of durability is becoming increasingly important for the concrete industry. This will apply to both design of new structures and assessment of existing structures. The corrosion of reinforcement embedded in concrete, caused by chloride ingress from marine exposure or from de-icing salts, is one of the most onerous degradation mechanisms that exist. The normal procedure to obtain sufficient durability is to ensure a minimum concrete quality combined with a minimum cover thickness. With the use of performance based material design it is possible to obtain better sustainability and to tailor-make the concrete structures to the actual use. This paper presents a novel design diagram that takes all the important exposure and material parameters into account.

Key words: Chlorides, Corrosion, Service life, Performance based design, Sustainability.

1. INTRODUCTION

There is an ongoing trend for performance based durability design of concrete structures, which is dictated partly by the industry's wish to increase its competitiveness and innovativeness and partly by the general quest for increased sustainability in the construction sector. One of the major buzz-words for the concrete industry is the excellent durability and the long service life of concrete. In the coming revision of Eurocode 2, performance based durability design is to be introduced instead of the current prescriptive deemed-to-satisfy-based concept. The author is participating actively in this revision work together with other European experts.

The main purpose of this paper is to introduce a simple illustrative concept based on the *fib* service life design model for chloride ingress [2,3]. There is an urgent need to teach the basic durability concepts to the designers and engineers in order for them to be able to understand and implement the performance based design principles correctly. At present the normal durability design process is limited to prescribing appropriate exposure classes and prescribing the associated minimum cover thickness. All material related issues are normally left to the concrete manufacturer according to the deemed-to-satisfy requirements given in EN 206 [1] together with national provisions. In the performance based design concept it is expected that the concrete manufacturer documents and produces various concrete qualities complying with various material resistance classes. Each resistance class needs to be documented via standardised testing which is defined in the relevant concrete standards. This could include testing of chloride migration resistance, freeze-thaw scaling, carbonation rate, etc. For durability issues regarding reinforcement corrosion Fig. 1 shows the performance based principle where a trade-off between lower material resistance and higher cover thickness and vice versa is possible.

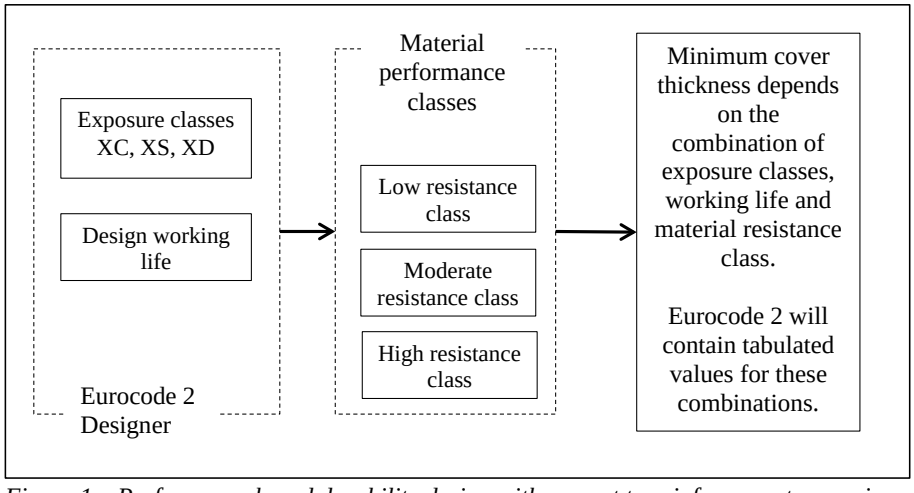

Figure 1 – Performance based durability design with respect to reinforcement corrosion.

2 MODEL FOR CHLOIRIDE INGRESS

2.1 Theoretical background

The normal approach to model chloride ingress with time t is to use the error function solution to the Fick's 2nd law for one-dimensional diffusion [2]:

$$C(x,t) = C_s - (C_s - C_i) \cdot \text{erf}\{Z(x,t)\}, \text{ where } Z(x,t) = {}^{x}/_{\left(2\sqrt{D_{app}(t) \cdot t}\right)} \quad (1)$$

Where C denotes the chloride ion concentration at depth x from the exposed surface. Index i denotes initial concentration in the mix at time t=0 and index s denotes the constant surface concentration at x=0. D_{app} is the apparent diffusion coefficient at time t. It is generally accepted that the diffusion coefficient decreases with the age of the concrete for several years. This is especially pronounced for binder combinations with supplementary cementitious materials such as PFA or GGBFS [2,3,4]. The diffusion coefficient is normally given in the unit 10^{-12} m^2/sec = µm^2/sec and sometimes the unit mm^2/year = 31.7 µm^2/sec is also used. Due to the limited number of pages it is not possible to describe the apparent diffusion coefficient further here.

The limit state used to determine the anticipated design service life T is governed by the chloride concentration, at the depth of the reinforcement (x=c), reaching a critical level C_{crit}. Hence, the limit state function $C(x=c, t=T) \leq C_{crit}$ is inserted in (1), yielding:

$${(C_s - C_{crit})}/{(C_s - C_i)} \leq \text{erf}\{Z(c,T)\} = \text{erf}\left\{\frac{c}{D_{app}(T) \cdot T}\right\} \quad (2)$$

The left hand side represents the load of the chloride exposure on a non-dimensional scale from 0 to unity. The right hand side is the resistance function. By choosing proper partial factors on load and resistance the safety level may be calibrated to an acceptable probability of failure. Both the surface concentration C_s and the critical concentration C_{crit} are subject to large scatter and many complicated models are proposed over the years [5-8] taking into account binder type and exposure conditions. It is outside the scope of this paper to describe these models.

2.2 Diagram for assessment of service life design

Figure 2 contains a diagram that makes it fairly easy to assess the impact of a certain parameter in (2). The range of parameters shown in the diagram is valid for most scenarios. The diagram is used by following the dashed line from (a) to (f) according to the following scheme:

a. Start by choosing the surface concentration C_s in weight-% of the concrete weight.
b. The critical threshold concentration of chlorides C_{crit} (in weight-% of binder weight) is found by the solid lines.
c. The corresponding value of the error function is found on the curve and the line continues vertically into the lower part of the diagram.
d. The lower left part of the diagram contains the apparent diffusion coefficient D_{app} at the time of expected service life.
e. The desired service life curve is found in the lower right part of the diagram.
f. Finally the necessary minimum cover thickness is read on the horizontal axis to the right.

3 CONCLUSION

The design of concrete structures is expected to be optimised with respect to durability and performance. Therefore, Eurocode 2 is being revised to deal with performance based durability design. However, in order to understand the concept of service life design and performance based material design it is important to educate the design engineers. This paper provides a fairly simple tool in order to do so. A novel easy to use diagram is presented, including the most important parameters used for design of cover thickness to meet a given service life under exposure conditions with chlorides. The large influence of the diffusion coefficient, the surface concentration of chlorides and the chloride threshold value is clearly seen from the diagram.

REFERENCES

[1] DS/EN 206: “Concrete – Specification, performance, production and conformity”, European Committee for Standardisation (2013)
[2] *fib*: “Model Code for Service Life Design” , fib Bulletin No 34, International Federation for Structural Concrete (fib), Lausanne, Switzerland (2006)
[3] Bamforth, P.B.: “Enhancing reinforced concrete durability: Guidance on selecting measures for minimising the risk of corrosion of reinforcement in concrete”, TR61, The Concrete Society, UK (2004)
[4] Skjølsvold, O.: “ Kloriddiffusjon i betong, Vurdering af aldringseffekt ved felteksponering”, COIN Report 11 (in Norwegian), SINTEF, Trondheim, Norway (2009).
[5] Sørensen, H. E., Poulsen, S. L. & Jönsson U.: ”Chloride threshold values from concrete blocks exposed at Rødbyhavn marine exposure site”, Proc. fib Symposium 2016, Cape Town, South Africa. (2016)
[6] Duracrete: “General guidelines for durability design and redesign”, BE95-1347, Brite EuRam III (2000)
[7] Maage, M., Helland, S., Poulsen, E., Vennesland, Ø. & Carlsen, J. E.: ”Service Life Prediction of Existing Concrete Structures Exposed to Marine Environment”, ACI Materials Journal, 93(6), 1-8 (1996)
[8] Frederiksen, J.M. & Poulsen, E.: ”Chloride penetration into concrete, Guide”, HETEK Report 123, www.hetek.teknologisk.dk (1997)

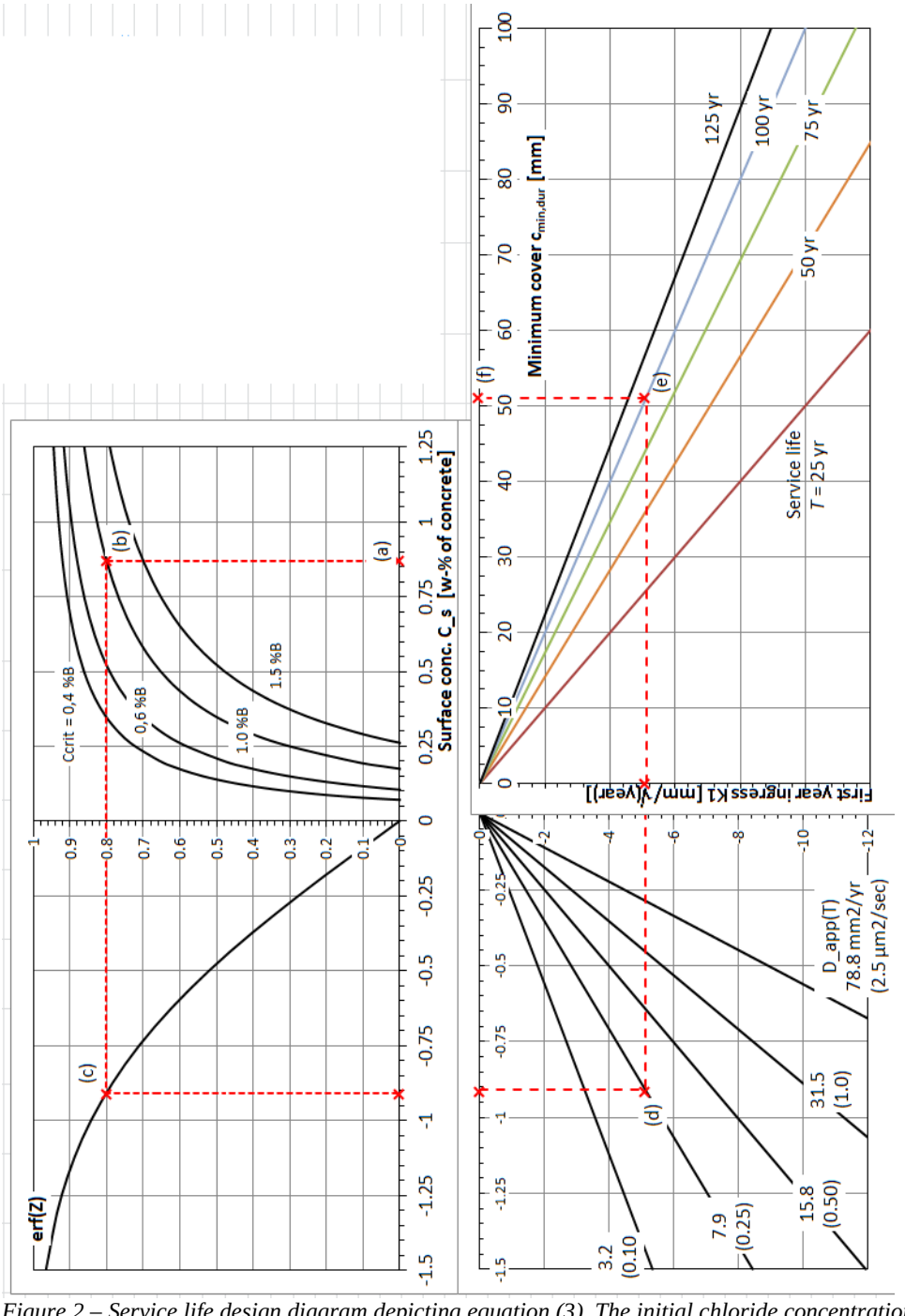

Figure 2 – Service life design diagram depicting equation (3). The initial chloride concentration C_i = 0.005 %B. The diagram is drawn for binder content of 400 kg/m^3.

Session A6:

AIR ENTRAINING AGENTS AND FROST ACTION

The air void contents effect on the salt frost scaling of uncarbonated concrete containing siliceous fly ash or slag

Martin Strand
M.Sc. PhD Student
Building Materials
Department of Building and Environmental Technology
Faculty of Engineering, LTH, Lund University
P O Box 188, SE-221 00 Lund, Sweden
Phone +46 46 222 4260
E-mail: martin.strand@byggtek.lth.se

Katja Fridh
M.Sc., PhD., Supervisor
Building Materials
Department of Building and Environmental Technology
Faculty of Engineering, LTH, Lund University
P O Box 188, SE-221 00 Lund, Sweden
Phone +46 46 222 3323
E-mail: katja.fridh@byggtek.lth.se

ABSTRACT
The first half of this PhD project has analysed the effect various air void contents has on the mass of de-icing salt frost scaling (DISFS) of uncarbonated concrete containing siliceous fly ash or slag. This has been done by finding a combination of air entraining agent and superplasticizer for each binder combination that has been used to enable the creation of various air void contents. Then the concrete has been cured moisture sealed for 307 days hydrated before the DISFS test began. The results show that the DISFS resistance vary between the different binders and the air void content clearly has various impacts on the DISFS depending on the binder combination.

Key words: Frost action, Supplementary Cementitious Materials (SCM), Testing, Admixtures, De-Icing Salt Frost Scaling

1. INTRODUCTION

To lower the energy consumption and carbon dioxide (CO_2) emissions from cement production fractions of the binder can be replaced with supplementary cementitious materials (SCMs) such as fly ash, slag and lime filler which has been used in this project. However, when adding these SCMs the hydration products and therefore final microstructure of the concrete changes in comparison to when only ordinary Portland cement is used [1]. This can affect the mass of de-icing salt frost scaling (DISFS) resistance of various concrete surfaces.

Two other factors which affect the DISFS of concrete is the air void system [2, 3] and preconditioning; carbonation [4], temperature and moisture history of the concrete test surface [5]. According to the theories and observations regarding the mechanisms of the DISFS in concrete containing 100% CEM I is that when creating an air void system (e.g. by including an air entraining agent (AEA)) in the concrete the mass of DISFS will decrease [2, 3]. However, it is uncertain if the air void system has the same effect when the concrete contain siliceous fly ash

(SFA) or ground granulated blast furnace slag (GGBFS) since the microstructure will differ. Therefore this project have tested concrete containing various fractions of SFA or GGBFS and made each recipe with 4 different air void contents. In addition to this, the DISFS test is split in to two different series. The first series is finished, where the concrete had hydrated for 307 days and never dried before the DISFS test began. Since it had never dried it can be assumed that the surface is uncarbonated. In the second large series samples from the same casts will be tested. These samples have hydrated for the same time, however then they have dried and carbonated in 20 °C and 60% RH for approximately 700 days before the test start. This study will therefore result in more information regarding how the mass of DISFS varies for concrete containing different binder combinations and how various air void systems affect these. The present article will present some of the results from the first series which have tested the never dried and therefore uncarbonated test surfaces.

2. MATERIALS

One type of ordinary Portland cement (CEM I) is used in all recipes, one type of siliceous fly ash is used and one type of ground granulated blast furnace slag is used. The name of the cement, according to the European standards [6], is CEM I 42,5 N - SR 3 MH/LA. Table 1 present each binder combination that has been tested.

Table 1 – Binder combinations used in the studies.

Binder	Abbreviation
100% CEM I 42,5 N - SR 3 MH/LA	CEM I
80+20 mass% CEM I + SFA	F20
65+35 mass% CEM I + SFA	F35
80+20 mass% CEM I + GGBFS	S20
65+35 mass% CEM I + GGBFS	S35
30+70 mass% CEM I + GGBFS	S70
65+25+10 mass % CEM I + GGBFS + LF	K35

The project also tested three air entraining agents and five superplasticizers to find one combination of AEA and SP which work well together with each binder combination. When one combination of AEA and SP had been found for each binder combination, four air void systems were created by varying the mass of AEA.

3. RESULTS

To get an indication of the air void system inside the casts air void analysis was made on one sample (100x150 mm²) per cast with linear traverse according to the standard [7]. When varying the mass of AEA the air void analysis showed that the amount of small air voids increased according to Table 2.

Table 2 – Air voids <0.35 mm in the paste for each binder combination and each cast

	Air voids <0.35 mm in the paste [%]						
Cast	CEM I	F20	F35	S20	S35	S70	K35
1	2,8	0,9	1,0	2,2	1,5	2,6	3,0
2	2,8	2,6	2,2	3,0	3,9	3,2	3,5
3	3,9	3,3	4,7	3,7	4,3	4,1	4,5
4	5,7	5,9	5,8	6,1	6,7	3,5	4,9

The increase in small air voids was expected when increasing the mass of added AEA. Other results from the air void analysis did not show the same consistency, e.g. spacing factor and specific surface presented in Table 3. These results would most likely show a clearer trend (e.g. smaller spacing factor with increasing AEA) if more samples, i.e. larger total surface area, had been analysed with linear traverse from the same casts.

Table 3 – Air content in the concrete for each binder combination and each cast

	Specific surface [mm^{-1}]						
Cast	CEM I	F20	F35	S20	S35	S70	K35
1	16	6	15	9	8	13	14
2	17	23	13	10	16	17	15
3	20	15	30	22	22	14	20
4	20	21	19	27	18	15	22
	Spacing factor [mm]						
Cast	CEM I	F20	F35	S20	S35	S70	K35
1	0,43	1,00	0,53	0,66	0,75	0,52	0,45
2	0,40	0,33	0,44	0,49	0,37	0,38	0,40
3	0,33	0,41	0,20	0,32	0,29	0,39	0,29
4	0,27	0,28	0,27	0,21	0,26	0,42	0,28

Figure 1 and 2 present the accumulated scaling after 56 cycles for the different binder combinations. Each binder combination has four bars that present the different casts with different masses of AEA that created four different air void systems with an increased amount of small air voids.

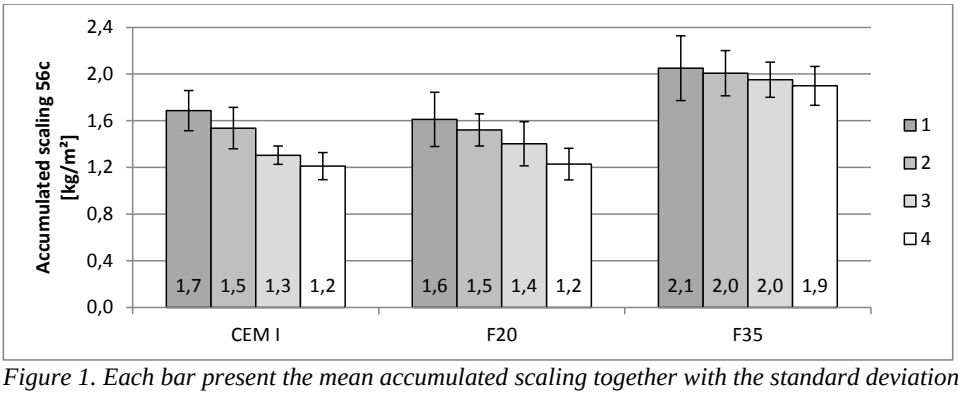

Figure 1. Each bar present the mean accumulated scaling together with the standard deviation for 6 samples after 56 cycles. Cast #1 contained 0 g AEA and cast #4 contained the largest mass of AEA.

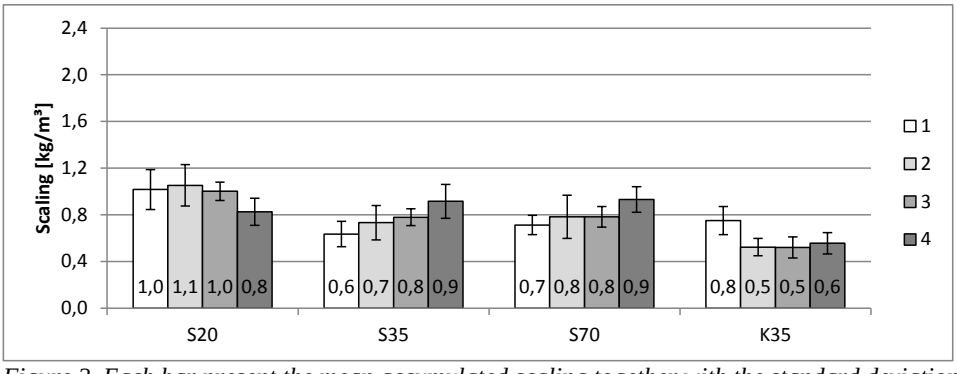

Figure 2. Each bar present the mean accumulated scaling together with the standard deviation for 6 samples after 56 cycles. Cast #1 contained 0 g AEA and cast #4 contained the largest mass of AEA.

4. CONCLUSIONS

Here are some of the conclusions drawn so far from the DISFS test results.

- The various binder combinations that have been tested produce various masses of DISFS which mean that the differences in the structure and properties between them could contribute to resisting the DISFS mechanism to various extents.
- An increased amount of small air voids in the hardened cement paste has various effects on the mass of DISFS for the various binder combinations.
    - There seems to be a consistent decrease in mass of DISFS with an increased amount of small air voids for CEM I and CEM I + siliceous fly ash concrete.
    - The concrete containing CEM I with GGBFS seems to generally have a lower mass of scaling, however the recipes does not seem to gain the same consistent effect as the concrete with SFA from the increased amount of small air voids.

REFERENCES

[1] K., B.E.S., *Evolution of pore structure in blended systems.* Cement and Concrete Research, 2015. **73**: p. 25-35.

[2] Valenza II, J.J. and G.W. Scherer, *A review of salt scaling: II. Mechanisms.* Cement and Concrete Research, 2007. **37**(7): p. 1022-1034.

[3] Powers, T.C., *The mechanism of frost action in concrete (Part II).* Cement, Lime and Gravel, 1966. **41**(6): p. 5.

[4] Utgenannt, P., *The influence of ageing on the salt-frost resistance of concrete*, in *Department och Building and Environmental Technology*. 2004, Faculty of Engineering, LTH, Lund University: Lund. p. 346.

[5] Sellevold, E.J. and T. Farstad, *Frost/Salt-testing of Concrete: Effect of Test Parameters and Concrete Moisture History.* 1991.

[6] 197-1, S.-E., *Cement - Part 1: Composition, specifications and conformity criteria for common cements*. 2011. p. 48.

[7] ASTM, *ASTM C457 / C457M - 12, Standard Test Method for Microscopical Determination of Parameters of the Air-Void System in Hardened Concrete*. 2012.

The influence of carbonation and age on salt frost scaling of concrete with mineral additions

Ingemar Löfgren, PhD
Thomas Concrete Group AB, 402 26 Gothenburg, Sweden
ingemar.lofgren@thomasconcretegroup.com

ABSTRACT
Resistance to salt frost scaling is tested by accelerated methods such as CEN/TS 12390-9. However, it has been shown that ageing and coupled deterioration mechanisms, like carbonation or leaching, can alter the frost resistance e.g. for concrete with high amount of slag (GGBS). This paper presents results from a laboratory study of concrete which have been exposed to accelerated carbonation at 1% CO2-concentration at different ages. The results show that exposing the specimens to accelerated carbonation at a young age result in an increased scaling and a carbonation depth corresponding to 10 year natural exposure. By increasing the age before the accelerated carbonation exposure the scaling is significantly reduced and the salt frost scaling resistance correlates better with field observations.

Key words: Frost action, Carbonation, Supplementary Cementitious Materials (SCM), Testing.

1. INTRODUCTION

The resistance of concrete to salt frost scaling is tested by accelerated methods such as CEN/TS 12390-9 [1] and SS 137244 [2], which originally were developed based on the experience of Portland cement concrete [3] [4]. The testing regime is being under review, partly due to that it does not consider ageing effects, such as changes to pore structure, micro cracking, leaching and the effect of carbonation [3] [4] [5]. With increasing use of mineral additions, such as slag (GGBS) and fly ash (FA), for reducing the environmental footprint and improve resistance to reinforcement corrosion this type of test methods need to be modified so that it can safely and adequately be used for concrete with mineral additions. Moreover, the test results also need to be correlated with the performance in field conditions [6] [7] [8].

2. EXPERIMENTAL PROGRAMME

The concrete mixture proportions are listed in Table 1. The aggregate was of granitic type, the superplasticizer (SP) was polycarboxylate-based (PCE), and the air entraining agent was a synthetic surfactant. The concrete had w/b ratio of 0.45 or 0.40 and had GGBS additions from 20 to 60 % of the total binder content. For additional mixes and results see [9].

Table 1 - Investigated concrete mixes.

Mix ID	Cement	GGBS	*w/b*	Air content
CEM I 0% 0.45	CEM I 42,5 N SR3 MH LA	0 %	0.45	5.2 %
CEM I 20% 0.45	CEM I 42,5 N SR3 MH LA	20 %	0.45	4.9 %
CEM I 30% 0.45	CEM I 42,5 N SR3 MH LA	30 %	0.45	5.1 %
CEM I 40% 0.45	CEM I 42,5 N SR3 MH LA	40 %	0.45	5.0 %
CEM I 60% 0.45	CEM I 42,5 N SR3 MH LA	60 %	0.45	5.8 %
CEM I 0% 0.40	CEM I 42,5 N SR3 MH LA	0 %	0.40	5.5 %
CEM I 20% 0.40	CEM I +20%S	20 %	0.40	6.0 %
CEM I 30% 0.40	CEM I +30%S	30 %	0.40	6.2 %
CEM I 40% 0.40	CEM I +40%S	40 %	0.40	6.2 %

The standard slab test procedure for freeze-thaw testing as described in CEN TS 12390-9 [1] and SS 137244 [2] were used to assess the salt-frost scaling resistance on a cut surface. Four different preconditioning regimes have been studied:

- **Standard procedure - 31d Std:** From demoulding (24±2 h) the cube is stored in water until the age of 7 days, and then stored in climate chamber (20±2°C and RH 65±5%) until a 50 mm thick specimen is cut at an age of 21 days. The slab is placed in a climate chamber (20±2°C and RH 65±5%) until it is 28 d old. At 28 d, 3 mm de-ionized water is poured on the top surface and the specimen is saturated for 72±2 h. At the age 31 d the freeze thaw cycles are started.
- **Modified standard procedure – 31d C:** As standard procedure, but from the age 21 d until 28 d the cut specimen is placed in a climate chamber with 1.0 % CO_2-concentration (20±2°C and RH 65±5%). At 28 d, 3 mm de-ionized water is poured on the top surface and the specimen is saturated for 72±2 h. At the age 31 d the freeze thaw cycles are started.
- **45 d curing regime – 45d C:** From demoulding (24±2 h) the cube is stored in water until the age of 21 days. Then the cube is stored in a climate chamber (20±2°C and RH 65±5%) until specimen is cut at an age of 35 days. At the age 35 d the cut specimen is placed in a climate chamber with 1.0 % CO_2-concentration (20±2°C and RH 65±5%) until it is 42 d old. At 42 d, 3 mm de-ionized water is poured on the top surface and the specimen is saturated for 72±2 h. At the age 45 d the freeze thaw cycles are started.
- **87 d curing regime – 87d C:** From demoulding (24±2 h) the cube is stored in water until the age of 63 days. Then the cube is stored in a climate chamber (20±2°C and RH 65±5%) until specimen is cut at an age of 77 days. From the age 77 d until 84 d the cut specimen is placed in a climate chamber with 1.0 % CO_2-concentration (20±2°C and RH 65±5%). At 84 d, 3 mm de-ionized water is poured on the top surface and the specimen is saturated for 72±2 h. At the age 87 d the freeze thaw cycles are started.

For all specimens, the weights were recorded immediately before and after the saturation with de-ionized water to determine the water uptake. Moreover, on accompanying specimens, cured in the same manner as the specimens for freeze-thaw testing, the carbonation depth was determined after 7, 14 and 28 d exposure to 1.0% CO_2 by spraying a phenolphthalein solution on a freshly split concrete surface. In addition, the compressive strength of the concretes were determined at 28, 56, and 180 days, see [9].

3. RESULTS AND DISCUSSION

The surface scaling after 56 cycles are presented in Figure 1. The acceptance criteria for "good" frost resistance according to SS 137244 [2] is shown in the figure. As can be seen in the figures, in all cases the scaling compared with the standard procedure increased for the carbonated specimens independent of curing condition, with the exception of mix C+20%S 0.40 for 45d C and 87d C curing. The increase in scaling is generally highest for 31d C, i.e. when carbonation starts on specimens at an age of 21 d. In Figure 2 the carbonation depth for the different concrete mixes and curing conditions are presented. The carbonation depths are, as expected, influenced by the curing conditions and age at exposure and are lower for more mature specimens. Moreover, with increasing GGBS content the carbonation depth increase and with decreased *w/b* ratio it decreases and is considerably lower, especially for the more mature specimens (curing condition 87d C). With respect to the measured carbonation depths for the accelerated carbonation (7 days in 1% CO_2) the measured depths should be compared to what is expected in field conditions (exposure conditions corresponding to XF4). Data from specimens exposed to atmospheric CO_2 during 11 year exposure at a field stations [8] showed a carbonation depth of about 1.1 mm with 30% GGBS at *w/b* 0.50 and 3.8 mm for a CEM III/B at *w/b* 0.50. At *w/b* 0.40 the carbonation depths were approximately 0.7 mm respectively 2.1 mm.

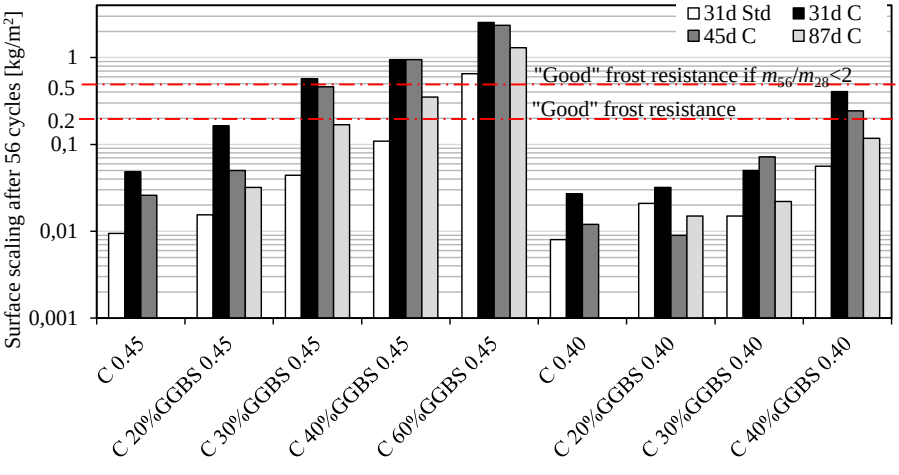

Figure 1 -. Comparison of the surface scaling (log scale) after 56 cycles.

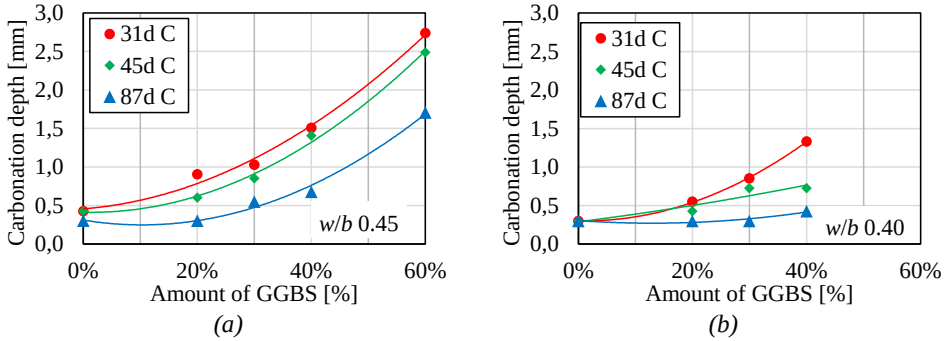

Figure 2 - Comparison of carbonation depth after 1 week in 1% CO2 for the different curing conditions for w/b 0,45 (a) and w/b 0.40 (b).

4. CONCLUSIONS

The effect of accelerated carbonation, 1 week with 1% CO2-concentration, on salt-frost scaling and the influence of different curing conditions has been studied. With the materials used and *w*/*b* ratios investigated it is clear that at 20% GGBS of total binder there is very little effect of carbonation on the frost resistance. Even with early accelerated carbonation at age of 21 days (31d C) all the tested concretes meet "good" scaling resistance or better after 56 cycles. For higher amounts of GGBS the early accelerated carbonation lead to increased scaling and especially at high amounts of GGBS (>40%). For the longest curing time 87d C (77 days when starting carbonation) the scaling was lower and GGBS contents of 30% achieved good frost resistance, this was also the case for some of the mixes with 40% GGBS); however, the scaling was still higher than for standard testing procedure. It should be pointed out that for the mixes with a higher slag content the compressive strength was much lower as an efficiency factor (k-value) of 1.0 was used, see [9]. The following conclusions can be made:

- With 20% GGBS of the total binder it was found that carbonation did not have a significant effect on the salt-frost scaling, even at early age carbonation.
- A GGBS content of about 30 to 40% is reasonable with respect to the salt-frost scaling resistance, but the testing and carbonation should not be done to early as this will produce a carbonation depth corresponding to more than 10 years natural carbonation.
- A prolonged curing regime before commencement of carbonation is needed if the test results should be realistic. In this study an age of 77 days when starting carbonation and 87 for start of frost cycles seems to have given reasonable results.

ACKNOWLEDGEMENT

This project has been financially supported by the Swedish Transport Administration.

REFERENCES

[1] CEN/TS 12390-9, *Testing hardened concrete – Part 9: Freeze/thaw resistance – Scaling*.
[2] SS 137244, *Concrete testing- Hardened concrete- Frost resistance,* Swedish Standards Institution (SIS), 4th edition, Stockholm, Sweden 2005.
[3] Utgenannt, P., *The influence of ageing on the salt-frost resistance of concrete,* Report TVBM-1021, Division of Building Materials, Lund Institute of Technology, Lund, 2004.
[4] Rønning, T, *Concrete Freeze-Thaw Scaling Resistance Testing Experience and Development of a Testing Regime & Acceptance Criteria*, In Workshop Proc. 'Durability aspects of fly ash and slag in concrete' Nordic Miniseminar 15-16 Feb. 2016, Oslo.
[5] Ferreira, M., Leivo, M., Kuosa, H., Holt, E., *The effect of by-products on frost-salt durability of aged concrete*, In Workshop Proc. 'Durability aspects of fly ash and slag in concrete' Nordic Miniseminar 15-16 Feb. 2016, Oslo.
[6] Boos, P, Eriksson, B.E., Giergiczny, Z., & Härdtl, R., *Laboratory Testing of Frost Resistance – Do the Tests Indicate the Real Performance of Blended Cements?* In proc. from the 12th Int. Congress on the Chemistry of Cement, Montreal 8-13 July, 2007.
[7] Boyd, A.J. & Hooton, R.D., Long-Term Scaling Performance of Concretes Containing Supplementary Cementing Materials, *J. of Mat. in Civil Eng.*, Vol. 19, pp 820-825, 2007.
[8] Utgenannt, P., *Frost resistance of concrete - Experience from three field exposure sites*. In Workshop proc. no. 8: Nordic Exposure sites - input to revision of EN 206-1, Hirtshals, Denmark, Nov. 12-14, 2008.
[9] Löfgren, I., Esping, O., & Lindvall, A., *The influence of carbonation and age on salt frost scaling of concrete with mineral additions*. International RILEM Conference MSSCE 2016, 22-24 August 2016, Technical University of Denmark, Lyngby, Denmark.

Effect of AEA-SP dosage sequence on air content and air void structure in fresh and hardened fly ash mortar

Andrei Shpak
PhD student
Norwegian University of Science and Technology,
Richard Birkelands vei 1a, NO-7034 Trondheim
e-mail: andrei.shpak@ntnu.no
Marcin Turowski, MSc, Norwegian University of Science and Technology
Ole Petter Vimo, BSc, Norwegian University of Science and Technology

Stefan Jacobsen
MSc, PhD, professor
Norwegian University of Science and Technology,
Richard Birkelands vei 1a, NO-7034 Trondheim
e-mail: stefan.jacobsen@ntnu.no

ABSTRACT
Laboratory measurements show that varying the dosage sequence of air-entraining agent and co-polymer in the mix (SP added before, after or together with AEA) greatly affects air entrainment in fresh and hardened fly ash mortar. Image analysis shows a good correlation between total air content and the air void spacing factor, though with a somewhat lower specific surface when SP is added together with AEA. Foaming measurements on the same materials and dosage sequences were therefore found less useful for studying the effect of admixture combinations. More work, including AVA measurements, is in progress to learn how to combine AEA, SP and fly ash in concrete.

Key words: Admixtures, Fly ash, Air entrainment, Testing.

1. INTRODUCTION

1.1 General

Production of frost durable fly ash (FA) concrete with a stable and protective air void system has often proven to be difficult. The problem has been ascribed to the variable carbon content in the fly ash causing variations in the required dosage of air entraining agent (AEA). Trial mixing to ensure quality output is therefore unavoidable even for batch-to-batch variations in fly ash.
The problem can hypothetically be resolved by reducing the number of sorption sites on carbon before the AEA encounters them. We think superplasticizer (SP) could block AEA access of AEA to some carbon in one of the AEA-SP combinations. Previous measurements have shown large effects on foaming in cement-fly ash water slurries of various SP/AEA combinations and dosage sequences [1]. The foam study indicated that a combination with SP drastically affects the adsorption kinetics. The same materials from the foam study [1] were also used to study the effect of addition of the admixtures on air entrainment [2].
The sequence of the addition of SP and AEA in concrete has been debated among practitioners for a long time, but the authors know of no experimental studies of SP-AEA dosage sequence in fly ash concretes in the literature. For regular OPC concrete, some authors [4], with reference to [7], suggest adding AEA after blending SP in the mix to give a stable air-void spacing factor; others [3] say that SP should be added after AEA, providing time for AEA to precipitate. No *standards*, *committees*, or *guidelines* specify the AEA-SP interaction. *In the industry*, SP-AEA dosage sequence practice varies due to the limitations of the concrete plant, economic reasons, or the producer's or client's established practice. The concrete producers reviewed recommend

that AEA is added either before or simultaneously with SP in the concrete mixes containing either pre-blended or separately added FA. The need for real knowledge about AEA and SP interaction in FA concrete is growing with the increased need for high volume fly ash concrete. *The scope of this work* was to investigate air void content and structure from laboratory mortar mixes where both the type of AEA and the dosage sequence of AEA- and a co-polymer SP were varied.

2 EXPERIMENTS

2.1 Mixing sequences and materials

Table 1 shows the 5 (five) admixture combinations and mixing sequences chosen based on experience with Foam Index testing:

Table 1 – Admixture combinations and mixing sequences.

Series ID	Admixture	Mixing sequence
	No admixture	1 min dry materials, 3 min water
1	Only AEA	1 min dry materials, 3 min water+AEA
2	AEA then SP	1 min dry materials, 2 min water+AEA, 1 min SP
3	SP then AEA	1 min dry materials, 1 min ½ water+SP, 2 min ½ water+AEA
4	SP with AEA	1 min dry materials, 3 min water+AEA+SP

2.2 litre mortar mixes were prepared in a Hobart table mixer. The volume fractions of filler-modified paste (all liquid, admixture, binder and mineral filler with particle size < 125 microns) were 330 and 400 litres/m^3 mortar, corresponding to normal and rich concrete mixes. The w/(c+FA) ratio = 0.46 for the 400 series and 0.57-0.63 for the 330 series [2]. FA/(c+FA) = 0.35 for all mixes. Two different anionic AEAs were used: AEA5 was based on synthetic tensides and tall oil derivatives, whereas AEA4 was an olefin sulfonate. The SP was an acrylic polymer. The cement used was a CEM I with a Blaine of 396 m^2/kg, additional low lime fly ash with 1.74 % carbon and a Blaine of 334 m^2/kg, and a limestone filler with a Blaine of 362 m^2/kg was used. All powders were supplied by Norcem-Heidelberg in Brevik, Norway. For details about admixtures and powders, see [1]. The aggregate was NS3099 standard Norwegian granitic 0-8 mm sand supplied by Norsk Stein Årdal.

2.2 Fresh and hardened mortar measurements

In the fresh mortar, the following measurements were made for each series: slump (40/80/120 slump cone on plexiglass plate) after 5 minutes, density after 8 minutes, pressure meter (1 L for mortars) after 9 minutes, and casting of 3 specimens 40 x 40 x 160 mm^3. All the mixes for AEA5 were reproduced at least twice, whilst mixes with AEA4 were made once.

In the hardened mortar, we measured the total air content from the demoulding density and using the PF-method, and air void parameters using image analysis (IMA) [6]. The samples were polished, inked, air voids filled with 2-4 μm $BaSO_4$ powder, scanned, and analysed after 90-120 days of storing in water.

3 RESULTS AND DISCUSSION

3.1 Fresh mortar measurements

Table 2 shows the 5 (five) different mortar mixes and their workability values.

Figure 1 shows the effect of AEA-SP dosage sequence on the total air content in the fresh mortar, when the dosage of AEA [% of binder] is held constant, and the corresponding Foam Index (FI) values from [1] with the same binders and admixtures. For the mixing sequences 2-4, the workability was kept constant at 60±10mm for the 330 series and 100±10mm for the 400 series respectively. FI measurements in squares above the bars show either the number of drops of SP to stop foaming or the time in seconds of stable foam (with a requirement at 45 sec).

Table 2 – Properties of the fresh mortar.

Mix	Paste volume, L [2]	w/b	Type of AEA*	AEA, [% (c+FA)]	SP, [% (c+FA)]	Slump [mm]
330	359	0.57	-	0	0	30
330	319–326	0.60–0.63	AEA5	0.7	0-0.20	20-60
400	371	0,46	-	0	0	20
400	346–373	0.46	AEA5	0.7	0-0.45	30-100
400	325**–370	0.46	AEA4	0.7	0-0.45	25-105

* AEA4 – Olefin sulfonate, AEA 5 – based on synthetic tensides and tall oil derivatives.

** 325L for series 4 (see Table 1), while series 1–3 range from 353L to 370L.

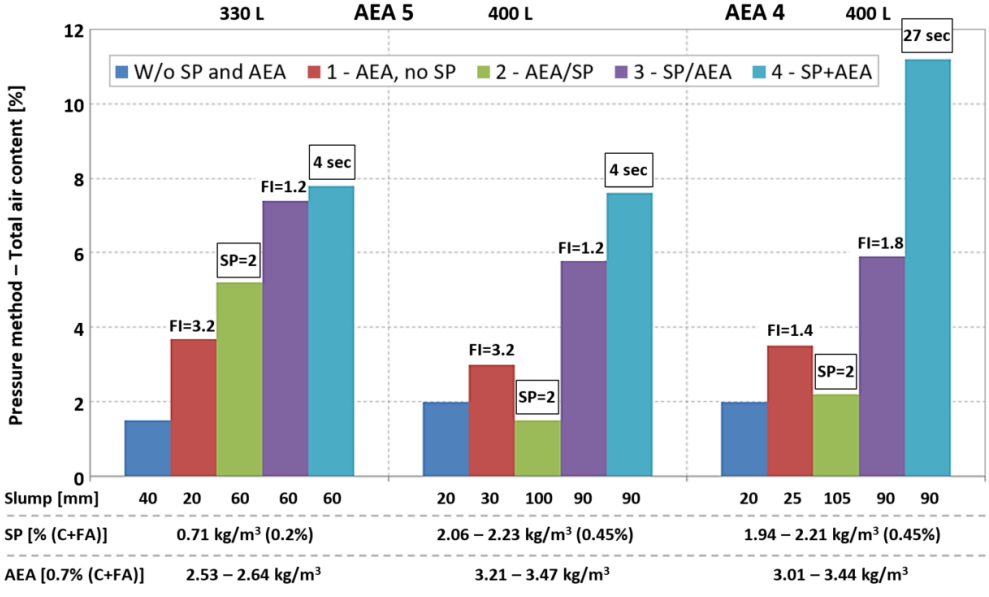

Figure 1 – Comparison of pressure meter results with FI measurements, Jacobsen et al. [1] for different matrix volumes and AEAs.

The results in Table 2 and Figure 1 show that both AEAs give big differences in air entrainment depending on the AEA-SP dosage sequence. The workability also affected air entrainment with some sort of reciprocal effect between air content and slump; most pronounced for AEA 5 when added first, see Figure1. The other series show negligible effect of workability. The highest amount of air voids is guaranteed by adding AEA and SP simultaneously (series 4), Eickschen E. and Müller C. [3] also mention this effect. When added together with SP, the pure synthetic surfactant AEA 4 shows a great contrast to the mixture of natural and synthetic components in AEA 5, but the difference is insignificant for other dosage sequences.

The results from foam index measurements do not fully reflect the properties of the mortar mixes, because this indicative test does not predict the development of the air-void system from the fresh to the hardened state. Furthermore, the very high air content when AEA and SP are added together does not correspond to the "foam killing" observed in [1]. Figure 2 shows that air content increased for series 2 (AEA before SP) meeting the requirements for the air void system, but in the fresh state (Figure 1) this combination was less promising.

3.2 Hardened mortar measurements

Mortar samples 160 x 40 x 40 mm were cast and split in two for hardened air-void analysis (IMA).

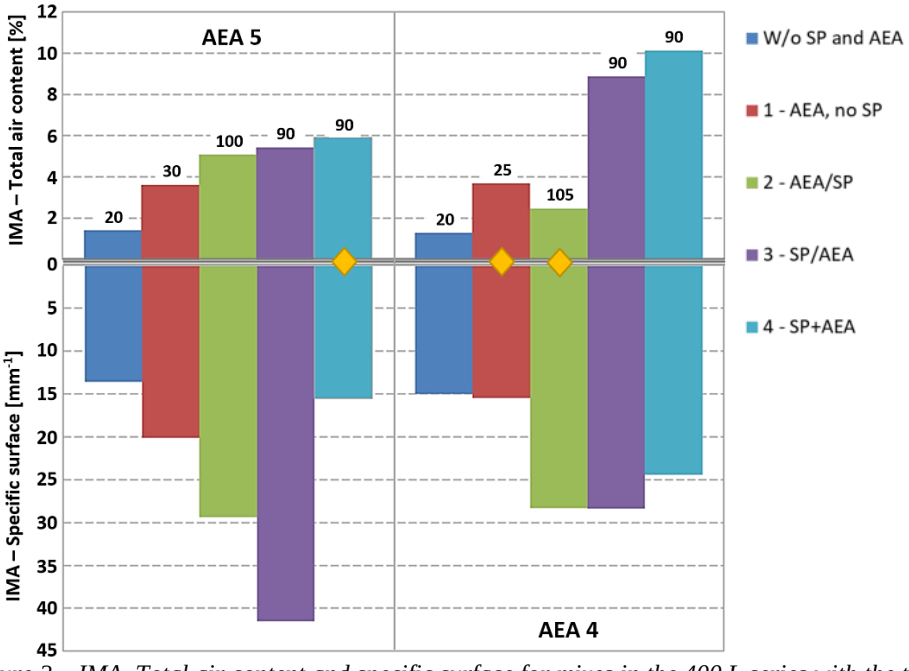

Figure 2 – IMA. Total air content and specific surface for mixes in the 400 L series with the two AEAs (the numbers over the bars show values for workability on 40/80/120 slump cone. Yellow rhombuses – done by a different operator)

Air void formation depends on several factors. Those that could possibly vary for mixtures with the two different AEAs are: the ratio of mixing time to activation time, and the susceptibility to coalescence and dissolution.
Further studies of fresh mortar with AVA are being carried out to study the impact of dosage sequence on air-void characteristics, including the ageing effect and the dosage for an acceptable air content and the resulting air void system.

REFERENCES

[1] Jacobsen S., Norhdahl H., Rasol H., Lødemel Ø., Tunstall L., Scherer G.W. Proc. MSSCE 2016 Frost Action in Concrete, Rilem Publications S.A.R.L., pp.61-70 (2016)
[2] Turowski M., Master thesis, NTNU, 64 p. (2016)
[3] Eickschen E., Müller C., Betontechnische Berichte 2010-2012, pp.41-58
[4] R. Rixom and N. Mailvaganam, 3rd Edition, E and FN Spon, London, 147 pp. (1999)
[5] Dodson, Vance H. “Concrete admixtures”, Ch 6: Van Nostrand Reinhold, NYC, (1990)
[6] Fonseca, P.C. & Scherer, G.W. Mater Struct 48: 3087-98 (2015).
[7] Freedman S., “High strength concrete” (1970). Modern Concrete. November. 170-6

ACKNOWLEDGMENT

This research forms part of the DACS project (Durable Advanced Concrete Solutions). The DACS partners are Kværner AS (project owner), Mapei AS, Multiconsult AS, NorBetong AS, NPRA (Statens vegvesen), the Norwegian University of Science and Technology (NTNU), and SINTEF Byggforsk. The project gratefully acknowledges the financial support of the Norwegian Research Council.

Stability of air-entrainment with PCE-superplasticizers

Fahim Al-Neshawy
D.Sc. (Tech.), Staff Scientist
Aalto University School of Engineering
Department of Civil Engineering
P.O.Box 12100, FIN-00076, Espoo, Finland
fahim.al-neshawy@aalto.fi

Jouni Punkki
D.Sc. (Tech.), Professor of Practice, Concrete Technology
Aalto University School of Engineering
Department of Civil Engineering
P.O.Box 12100, FIN-00076, Espoo, Finland
jouni.punkki@aalto.fi

ABSTRACT
Air content is an extremely important aspect of today's concrete performance and durability characteristics. Lately in Finland, elevated air contents (>15%) have been observed from the samples drilled from structures. The high air contents have caused deficiencies in the compressive strength of concrete structures.
One of the main factors affecting the stability of air content in concrete is the use of combination of Air-Entraining Agent (AEA) and Polycarboxylate Ether (PCE) –superplasticizers admixtures. This study is a part of research project, which investigate the stability of air-entrainment in concrete using different types of PCE-SP, AEA and concrete mix designs. The aim of the project is to achieve a stabile protective pore system for concrete.

Key words: Air content, Superplasticizer, Air-entraining, Admixtures, Cement, Mix Design.

1. INTRODUCTION

1.1. General.

Air content is an extremely important aspect of today's concrete mix design criteria and subsequent in-place concrete performance and durability characteristics. For example, the frost resistance of concrete is determined by the air-void system's ability to prevent the development of destructive pressures due to freezing and associated movement of moisture in the concrete pores. The specific requirements of the air-void system depend on the amount and movability of the water in the concrete pores.
Lately, elevated air contents have observed especially in bridges. Air contents exceeding 15% have been observed from the samples drilled from structures. In addition, low concrete densities (app. 2000 kg/m^3) have been measured from samples taken from close to the casting surface. One of the main factors affecting the stability of air content in concrete and thus is believed to be the use of combination of Air-Entraining Agent (AEA) and Polycarboxylate Ether (PCE) – superplasticizers admixtures. A research project "Robust Air – Securing the stabile protective pore system of concrete" for investigating the stability of air content in concrete was started in the beginning of 2017 at Aalto University, Finland. The research is still undergoing and we expect that the result will set requirements of the concrete mixtures so that a stabile protective pore system can be achieved.

1.2. Stability of air-content in concrete with superplasticizer

Lignosulphonates are generally regarded as '1st generation' superplasticizers, while the sulfonated melamine and sulfonated naphthalene are called '2nd generation', and the polycarboxylates and polyacrylates are termed as 3rd generation superplasticizers [1].

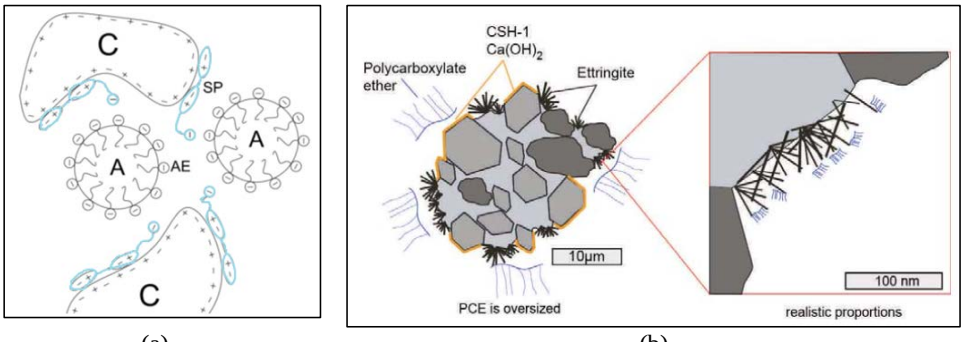

(a) (b)

Figure 1– (a) The mechanism of sulfonated based superplasticizer and air-entraining agent [2] and (b) the adsorbance of PCE superplasticizers in cement paste [3].

Eickschen and Müller (2015) investigated the action mechanisms occurring during the production of air-entrained concrete with different superplasticizers. The results show that the combinations of synthetic air-entraining agent and a PCE-based plasticizer exhibited a greater range of fluctuation in air content than combinations with natural air-entraining agents and conventional plasticizers.

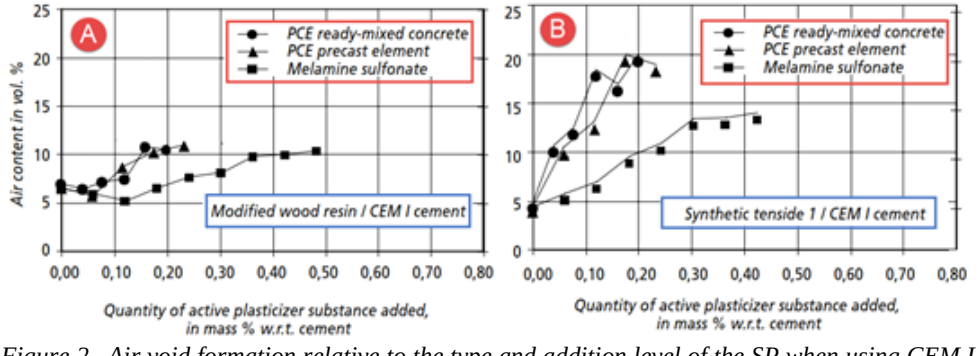

Figure 2– Air void formation relative to the type and addition level of the SP when using CEM I cement: (A) air-entraining agent based on wood resin, and (B) synthetic tenside 1 [4].

2. LABORATORY TESTING AND RESULT REPORTING

The aim of the project is to clarify the factors affecting the stability of the air entrainment. Both the effects of the concrete composition and admixture combination on the stability of the air entrainment are studied. Concrete tests with different types of AEAs and PCE- superplasticizers are carried out and the stability of entrained air is investigated. Admixture combinations from seven different admixture producers are investigated. All the superplasticizers tested are polycarboxylate ethers. Table 1 shows an example of the concrete mixtures.

Table 1 - Concrete mixtures with different strength classes, cement types, maximum aggregate size and consistency classes.

Concrete code	Cement, (kg)	Water, (kg)	Aggregates, (kg)	AEA/C, (%)	SP/C, (%)
45-PL-16-S3	425	140	1770	0.035	1.2
45-PL-16-F5	425	160	1716	0.035	1.2
45-PL-08-S3	440	155	1689	0.035	1.2
45-PL-08-F5	440	175	1636	0.033	1.2
37-PL-16-S3	400	140	1805	0.035	1.2
37-PL-16-F5	400	155	1765	0.035	1.2
45-SR-16-S3	425	140	1769	0.055	1.2
45-SR-16-F5	425	155	1729	0.054	1.2
45-BR-16-F5	425	155	1729	0.080	1.2

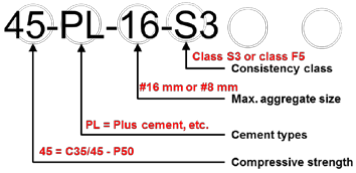

Effects of the variables mentioned on Table 1 on the air content of concrete at different moments after mixing are analysed. The air content is measured immediately after mixing, 30 min and 60 min after mixing. In addition, after 60 min superplasticizer is added to compensate the workability loss and air content is measured after 75 min after mixing. Also, the density variation of the concrete is monitored.

Figure 3 shows the effects of concrete properties on the air content of concrete as a function of time. Only one admixture combination is used in the these tests. The air contents have been calculated from the fresh concrete density.

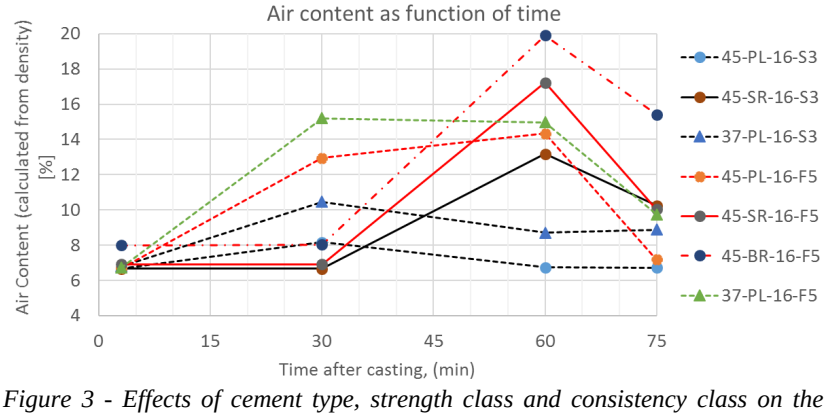

Figure 3 - Effects of cement type, strength class and consistency class on the air content of concrete as a function of time. The air content is calculated from fresh concrete density.

In most of the cases, the air content is significantly increasing after mixing either after 30 min or 60 min after casting. The lowest increase was taking place with concrete with moderate workability (Consistency class: S3). The highest increase took place with concrete having the consistency class F5. Against the assumptions, the air content was not increasing when superplasticizer was added to compensate the workability loss. In most of the cases, the air content was decreasing after 60 min (SP added after 60 min measurement). The air content of concrete was measured using both the pressure method and calculated from fresh concrete density. The correlation is relatively good until app. 10% air content, but with higher air contents the difference increases. It is not perfectly clear with method is better to measure the high air contents.

3. CONCLUSIONS

This paper is presenting the effect of the combination of Air-Entraining Agent (AEA) and Polycarboxylate Ether (PCE) –superplasticizers admixtures on the stability of the concrete air content. Based on the literature review, the practical experiences, and the portion of laboratory testing results in this paper, the phenomena of air content stability can be explained as follows:

1. If air entrainment “remains incomplete” during the mixing, air content will increase after mixing
2. The risk for elevated air content increases as:
    - Short mixing time, ineffective mixer
    - High dosages of SP and AEA
    - Synthetic AEA
    - High fluidity of concrete (taking into account the fine aggregate content)
    - Low cement and fine material contents

The research is still undergoing and the laboratory testing and result reporting will be completed during Spring 2017.

REFERENCES

[1] Whiting, D. and Nagi, M., (1998). Manual on Control of Air Content in Concrete. Portland Cement Association. Skokie, IL USA.

[2] Rath, S. and Ouchi, M. Effective Mixing Method for Stability of Air Content in Fresh Mortar of Self-Compacting Concrete in terms of Air Diameter. Internet Journal for Society for Social Management Systems Issue 10 Vol.1 sms15-6550 (2015)

[3] Wetzel, A., and Arend, J. Adsorbance of superplasticizers on concrete additives: microstructural in-situ experiments. 15th Euroseminar on Microscopy Applied to Building Materials • 17-19 June 2015 • Delft, The Netherlands (2015)

[4] Eickschen, E., Müller, C. Interactions of air-entraining agents and plasticizers in concrete. Concrete Technology Reports 2010 – 2012. VDZ gGmbH (Hrsg.). Düsseldorf, Germany. Online at: https://www.vdz-online.de/publikationen/betontechnische-berichte/ (2012).

Approach of an elevated criterion for frost resistance of concrete according to Estonian practice in concrete industry

Eneli Liisma
M.Sc., Ph.D. candidate, Teaching assistant
Tallinn University of Technology
Ehitajate tee 5, 19086 Tallinn
e-mail: eneli.liisma@ttu.ee

ABSTRACT
In general compressive strength of concrete is considered as the main characteristic to determine its potential in civil engineering. However, in a concept of concrete durability in northern countries, frost resistance is set as a parallel target to comply. The main focus of this article is to give an overview of Estonian practice in concrete industry with frost resistant concrete and its quality in two production intervals – during 2010 and 2016. Based on the results an elevated criterion and a preliminary gradual classification system for degradation evaluation are proposed for frost resistance of concrete.

Key words: Concrete, Freeze/Thaw, Evaluation, Production, Sustainability, Service Life

1. INTRODUCTION

Frost resistance of concrete is considered as a common durability concern with unstable climate conditions with a temperature alternating around 0^{o}C. In Estonia approximately 12-15 freeze/thaw cycles (FTC) result in a year. For comparison neighbouring-countries such as Finland and Latvia around 13 and 15 FTC are reported respectively. Although frost resistance of concrete is examined widely and general recommendations for concrete design towards freeze/thaw attack are compounded in EN 206, Annex F [1] e.g. minimum cement dosage or maximum water cement ratio. According to previous studies cement dosages from 300 kg/m^3 and above start to perform durable and stable result under FTC loads [2]. Water cement ratio from 0.55 and below reported to accomplish frost resistance. Yet degradation problems are noted to appear regularly. Based on variable research, one of the main influencer regulating frost resistance is considered proper air entrainment around 6% [2, 3]. Furthermore, spacing factor due to entrained air is reported to remain below 0.30 mm for frost resistance [4]. According to BY 65 Betoninormit [5] spacing factor is set to in compliance with exposure class and service life in a range of 0.22 and 0.30. Another aspect accomplishing frost resistance is the origin of coarse aggregate that is generally igneous type, mainly granite in Scandinavia with low capillary porosity (< 0.5%). However in Estonia limestone coarse aggregate as primal natural resource with higher capillary porosity (>1.0%) has relatively poor outcome as a compound of frost resistant concrete. Although limestone coarse aggregate is highly reduced in composition of frost resistant concrete in last years in Estonia due to increasing know-how and durability demands. This indicated to gather information of an overall quality status of frost resistant concrete in Estonia compared to half decade ago production. If there is a notable quality leap in concrete durability with frost resistance, an elevated criterion for frost resistance is an adequate and subsequent step. Contemporary evaluation approach according to EVS 814 is exposure class system related to scaling mass loss criteria from 0.20 kg/m^2 to 1.0 kg/m^2. Similar system

constructed by BY65 with frost resistance criterion from 0.20 to 0.50 kg/m^2. Degradation system from very good to acceptable or as mass loss from 0.10 kg/m2 to 1.00 kg/m^2 by Swedish SS 13 72 44 evaluation criteria.

2 EXPERIMENTAL SET UP

Ten concrete plants with their production were selected to analyze Estonian concrete quality subjected to frost resistance. 50% of the manufactures were micro producers in Estonian scale with < 10 000 m^3 year production and second half with > 150 000 m^3 year production. For a comparable purpose of presumable development of production technology in concrete industry in time, two production periods were taken into survey – 2010 and 2016. Three concrete classes in compliances with EVS-EN 206, Annex F [1] freeze/thaw attack exposure class recommendations were chosen - C30/37, C35/45 and C40/50. According to freeze/thaw attack exposure classes, both environmental factors were taken into investigation as de-icing agent – distilled water and 3% NaCl solution.

2.1 Specimen preparation

All specimens were prepared from constant production concrete and moulded in cubical moulds (150 x 150 x 150) mm according to EVS-EN 480-1 [6] procedure recommendations. Specimens were kept at relative humidity (95 ± 5) % and temperature (20^{o}C). Demoulding was performed after 24h and hardening was carried out at previous conditions before freeze/thaw testing.

2.2 Freeze/thaw test

Frost resistance of concrete was performed according to Estonian national standard EVS 814:2003 [7] that is mainly based on Swedish standard SS 13 72 44 [8] often referred as *Borås method.* Freeze/thaw cycles were accomplished by climate chamber Weiss Umwelttechnik GmbH WK3-340/40 and presented as a cumulative scaled material in kg/m^2.

3 RESULTS

Presumption of the study was set on potential development with frost resistance of concrete due to increasing know-how in concrete industry and material technology overall. Outcome of test results are presented in Figs. 1-3. As seen in Fig. 1 concrete class C30/37 comparable results exhibit an average scaling decrease with both de-icing agents. Average scaling (AS) in 2010 (marked with solid line) reached up to 1.5 kg/m^2 with distilled water after 56 FTC but must be noted that coarse aggregate was high porosity (>1.5%) limestone. However in 2016 limestone coarse aggregate was avoided and AS (marked with dotted line) after 56 FTC was significantly lower up to 0.10 kg/m^2. Similarly with 3% NaCl de-icing agent, comparable results indicated notable scaling decrease in 2016 nearly to 0.10 kg/m^2. Concrete C35/45 showed analogous trend as submitted in Fig. 2. With distilled water approximate result was accomplished. While in saline water AS decreased from 0.3 kg/m^2 to 0.1 kg/m^2 in selected years. As presented in Fig. 3 concrete class C40/50 gave very good results in distilled water with AS below 0.05 kg/m^2, though AS in saline water was just slightly over 0.20 kg/m^2 in 2016.

Considerable improvement in concrete durability during time can be brought forward comparing two constant concrete productions in Estonia selectively in 2010 and 2016. In Fig. 4 a preliminary approach of an elevated criterion and gradual degradation principle is presented.

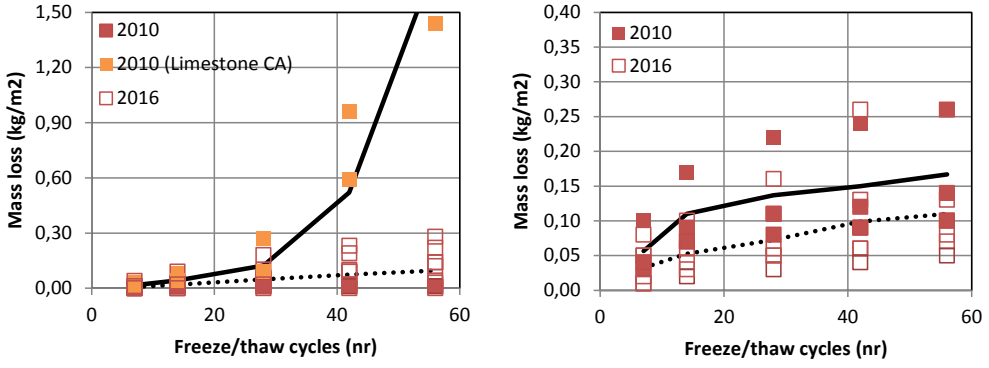

Figure 1 – C30/37 mass loss after FTC. Left: distilled water. Right: 3% NaCl.

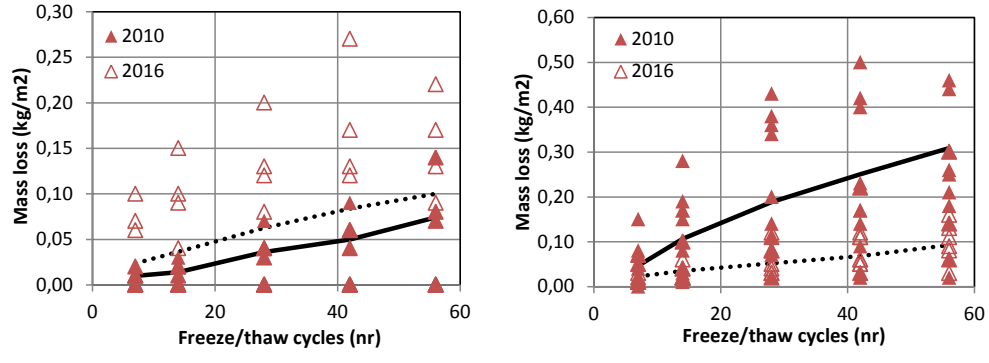

Figure 2 – C35/45 mass loss after FTC. Left: distilled water. Right: 3% NaCl.

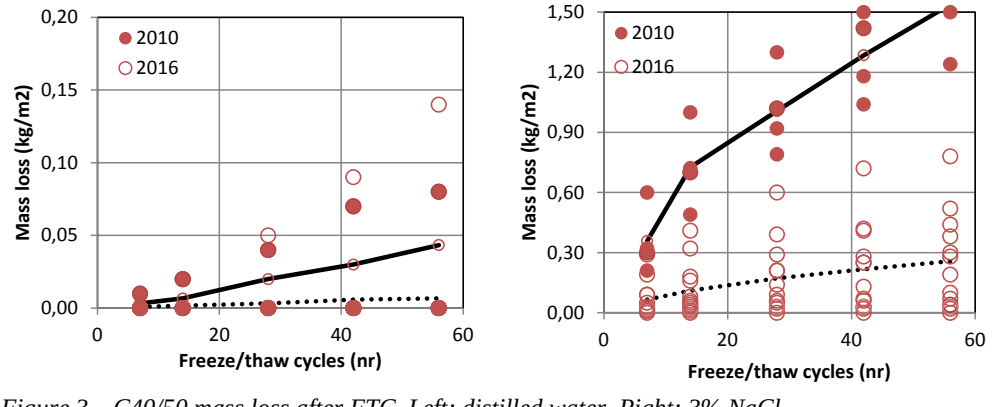

Figure 3 – C40/50 mass loss after FTC. Left: distilled water. Right: 3% NaCl

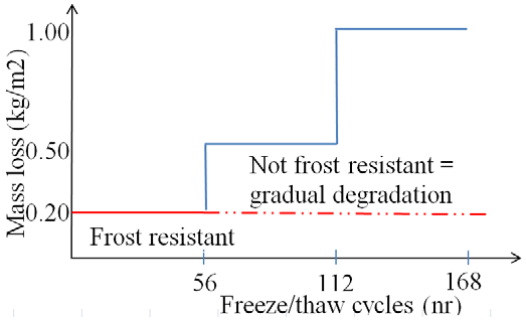

Figure 4 – Preliminary new approach of elevated criterion of frost resistance of concrete and gradual degradation principle.

4 CONCLUSIONS

According to constant concrete production in Estonia, a notable quality leap towards frost resistance of concrete can be brought forward during 2010 and 2016. This induces to maturity to elevate the criteria for evaluation frost resistance of concrete and renounce common exposure class relation to mass loss. In other words frost resistant concrete as a durable material should not have gradual evaluation principle as in EVS 814, BY65 but a fixed set target. Based on the results, a proposed set target for frost resistant concrete is 0.20 kg/m^2 after 56 FTC for all exposure classes. Proposed set target exceeded mass loss should not be considered as frost resistant concrete, thereupon characterized with gradual degradation class is acceptable.

ACKNOWLEDGEMENTS

This work was supported by institutional research funding of the Estonian Ministry of Education and Research IUT1−15 "Nearly-zero energy solutions and their implementation on deep renovation of buildings".

REFERENCES

[1] EN 206:2014+A1:2016: "Concrete – Specification, performance and conformity", Estonian Centre of Standardisation (2016)

[2] Penttala, V.; "Surface and internal deterioration of concrete due to saline and non-saline freeze/thaw loads" Cement and Concrete Research 36(5): 921-928 (2006)

[3] Ferreira, Kuosa, Leivo, Makkonen.: "The influence of frost attack on chloride transport in concrete": RILEM International workshop on performance-based specification and control of concrete durability: 159-166 (2013)

[4] Pinto, R.C., Hover, K.C.: "Frost and Scaling Resistance of High-Strength Concrete", Skokie, III: Portland Cement Association (2001)

[5] by 65 Betoninormit: BY-Koulutus Oy, Finland (2016)

[6] EN 480-1:2015: "Admixtures for concrete, mortar and grout – Test methods – Part 1: Reference concrete and reference mortar for testing", Estonian Centre of Standardisation (2015)

[7] EVS 814:2003: "Frost resistance of normal-weight concrete. Definitions, specifications and test method", Estonian Centre of Standardisation (2003)

[8] SS 13 72 44: 1995 "Betongproving – Hardad betong – Avfalning vid frysning. Concrete Testing – Hardened Concrete – Frost resistance" Standardiserings kommissionen i Svergie

Frost salt scaling of concrete

David Wahlbom, Ph.D. Student
Katja Fridh, Senior Lecturer
Division of Building Material
Faculty of Engineering, Lund University
Box 118, SE – 221 00 Lund, Sweden
david.wahlbom@byggtek.lth.se
katja.fridh@byggtek.lth.se

(Picture of main author David Wahlbom)

Teddy Feng-Chong, Senior Scientist
Patrick Dangla, Senior Scientist
IFSTTAR, Université Paris-Est
FR- 77420 Champs sur Marne, France
teddy.fen-chong@ifsttar.fr
patrick.dangla@ifsttar.fr

Mette Geiker, Professor
Stefan Jacobsen, Professor
Department of Structural Engineering
Norwegian University of Science and Technology
NO- 7491 Trondheim, Norway
mette.geiker@ntnu.no
stefan.jacobsen@ntnu.no

Jan Skocek
Ph.D., Senior Scientist at Global R&D
HeidelbergCement Technology Center
DE-69181 Leimen, Germany
Jan.Skocek@heidelbergcement.com

Quoc Huy Vu
Ph.D., R&D Project manager
LafargeHolcim
CH- 8645 Jona, Switzerland
quochuy.vu@lafargeholcim.com

ABSTRACT
The project will address the mechanism(s) of deterioration in frost salt scaling (FSS) including the potentially protective effect of entrained air voids and the performance of low-clinker blends. Frost deterioration of concrete is an important durability issue for concrete structures exposed to high humidity, frost and deicers (exposure classes XF1-4 in EN206). Today when the variety of binder compositions is rapidly increasing it is more important than ever to understand the mechanism behind the deterioration to define a reliable test method to obtain frost durable structures.

Key words: Frost Action, Concrete, Supplementary Cementitious Materials, Durability, Modelling, Cement.

1. INTRODUCTION

The combination of high degree of saturation and low temperatures can result in both surface scaling and internal cracking. Frost damage can lead to loss of concrete cover and thus reduced protection of the reinforcement and possible loss of bearing capacity. Frost damage in form of cracking facilitates ingress of aggressive substances and thus also other deterioration mechanisms. The degree of deterioration depends on the surrounding environment (such as temperature, precipitation, deicers, relative humidity) and the materials properties (such as permeability, pore size distribution, air void structure, and mechanical properties).

2. BACKGROUND

Long-term experience shows that concrete structures with high amounts of Portland clinker and various air entraining admixtures (AEA) can be durable. Field exposure investigations confirm that the existing test methods can usually predict the performance of Portland cement concrete [1]. However, with the increasing substitution of Portland clinker, problems with production (e.g. air entrainment, curing) and ageing (e.g. carbonation) of hardened concrete can lead to reduced protection. There are indications that low clinker concretes are less robust than PC concrete regarding placing and curing [2]. To solve these challenges improved understanding of basic mechanisms is needed.

Valenza and Scherer presented the Glue Spall theory explaining the mechanisms behind FSS [3]. The main features of this theory are that weak salt solutions on the concrete surface gives a weak ice layer during freezing depending on salt concentration. The ice has a larger thermal expansion coefficient than the concrete. Weak salt solutions will create a crack in the ice that will propagate into the concrete surface, causing the surface to be spalled off. The concrete can be protected by a proper air void system since this allows pore liquid to be sucked into and freeze in the air voids creating an additional contraction of the concrete surface as explained by Powers and Helmuth [4] and later described in a quantitative theory by Coussy [5]. This offsets the strain mismatch between the surface ice and concrete, hence reducing damage. Glue Spall theory tells us also that the higher the tensile strength of the concrete surface, the longer it can sustain the strain mismatch, and the lower the temperature the more cracking. If the concrete is not properly air entrained the thermal mismatch will cause spalling earlier, particularly in combination with internal frost damage [6]. The Glue Spall theory is the only model quantitatively explaining the pessimum effect of salt concentration and the impact of thickness of water layer on the surface. However, cycles, which could induce progressive air voids saturation and subsequent increased damage, are not considered. It indicates that positive effects of pozzolana are rather due to improvement of surface strength properties than improvement of transport properties and this has puzzled several researchers.

Fagerlund presented the theory of critical degree of saturation [7]. If a concrete has water content giving an actual degree of saturation higher than the critical degree of saturation and is exposed to freezing temperatures it will be severely damaged. Entraining air voids normally gives a reduced actual degree of saturation since the voids mainly stay dry. The critical degree of saturation is a material parameter individual for each concrete. Therefore, to make a prediction of the future service life possible one has to be able to predict the long term absorption into the air void system. Fagerlund presented a model of this long-term absorption based on dissolution and diffusion of entrapped air which will be replaced by water [8]. The model applies when the concrete is submerged. The main conclusion from Fagerlund's approach is that we have to consider air voids' size distribution, the smallest bubbles being rapidly saturated as air dissolution is fast. However, large air voids are almost never saturated. We should have in mind that the spacing factor is defined considering all the entrained air voids but progressive saturation starting with the smallest one, has the same consequence as increasing the spacing factor. Then even if we don't reach the critical spacing factor proposed by Fagerlund, as the spacing factor should exceed a certain limit, then the classical hydraulic pressure could build up again and generate expansion and damage even if the critical spacing factor proposed by Fagerlund is not reached. Fagerlund [9] has also proposed that pessimum salt concentrations can be due to a combination of osmotic pressure (increasing with salt concentration) and hydraulic pressure (reducing with salt concentration).

Lindmark [10] applied the theory of frost heave [11], on the surface of concrete – and could account for the same type of deterioration as Powers and Helmuth [4], [12]. This was called the theory of micro ice lens growth and when the critical degree of saturation was transgressed, the surface spalled off. If the concrete has an air void system with good spacing the ice in the air voids attracts the water and the resulting suction in the water offsets the tensile stresses created by ice lenses in the mesopores of the cement paste. Again this theory could be used to consider progressive air void saturation during cycles, taking into account permeability and other material properties. It is also interesting to notice that several researchers have established experimental correlation between FSS and surface sorption [13] which appears as another evidence of the impact of surface permeability, pore size distribution and their connectivity towards critical degree of saturation.

It is essential to recognize that more than one mechanism can contribute to surface damage and they can be more or less dominant under certain climatic conditions for materials with different properties. Another question lies in the mechanism at the origin of the potential beneficial effect of entrained air voids since Liu [13] found opposite results of Sun and Scherer [14].

To be able to obtain frost durable structures with a wider variety of binder compositions, we need a basic understanding of the FSS mechanism of concrete and an understanding why low clinker systems under some circumstances are more susceptible to FSS than PC. This information can be used to create improved experimental protocols to access sensitivity of low clinker systems to FSS.

3. SCOPE AND ACTIVITIES

The four main objectives of this research is first to model the key mechanisms involved in FSS covering the Glue Spall theory, water uptake by cryosuction, critical degree of saturation and repetitive cycles. The second objective is to define which material properties are decisive for resistance to FSS. The third objective is to determine the requirements for a protective air void structure, and the last objective is to establish an understanding of the impact of hydration and aging on FSS.

The main part of this project will be to extend the poroelastic model of cryosuction developed by Fen-Chong et al. [15] based on work by Coussy [5] to include influence of salt solutions and progressive air voids saturation during cycles as well as thermal contraction and surface properties related to the Glue Spall theory. A review of existing theories and parametric studies will be performed to identify the key parameters for frost scaling in the progressive saturation and Glue Spall theories.

ACKNOWLEDGEMENT

The work presented is being carried out at Division of Building Materials, Lund University Faculty of Engineering, LTH. The authors wish to express their acknowledgement to The Industrial-Academic Nanoscience Research Network for Sustainable Cement and Concrete, Nanocem and the Development Fund of the Swedish Construction Industry, SBUF for financing this project.

REFERENCES

[1] Utgenannt P, ‘Salt-Frost Resistance of Concrete Experience from field and laboratory investigations’ (presentation in the Nanocem frost workshop in Heidelberg 2015)

[2] Thomas M. Deicer Salt Scaling of Concrete Field Observations in North America’, (presentation in the Nanocem frost workshop in Heidelberg 2015)

[3] Valenza and Scherer, ‘A review of salt scaling: I. Phenomenology’, CCR 37, (2007), 1007-1021, Valenza and Scherer, ‘A review of salt scaling: II. Mechanisms’, CCR 37, (2007), 1022-1034

[4] Powers and Helmuth, ‘Theory of volume changes in hardened Portland-cement paste during freezing’, Proceedings, Highway Research Board 32,Bull. 46 (1953)

[5] Coussy, O., Mechanics and Physics of Porous Solids, Wiley, New York, (2010)

[6] Jacobsen S., Sellevold E.J. and Sæther D.H.: Frost testing high strength concrete: frost/salt scaling at different cooling rates, RILEM/Materiaux et Constructions, Vol.30, No. 195, Jan-Feb, 1997, pp. 33-42

[7] Fagerlund G, ‘The critical degree of saturation at freezing of porous and brittle materials’, Division of Building Materials, Lund University, Thesis, Report 34, (1972) 411 p.

[8] Fagerlund G, ‘The long time water absorption in the air pore structure of concrete’, Division of Building Materials, Lund University, TVBM-3051, (1993)

[9] Fagerlund G., Studies of the destruction mechanism at freezing of porous materials. Paper presented at the 6th international congress on problems raised by frost action. LeHavre April 23-25 1975, CBI report 1:76

[10] Lindmark, ‘Mechanisms of salt frost scaling of Portland cement-bound materials: Studies and hypothesis’, Doctoral thesis, Division of Building Materials, Lund Institute of Technology, TVBM-1017, (1998)

[11] Taber, ‘Mechanics of frost heaving’, Journal of Geology, 38, pp. 303-317, (1930)

[12] Powers, ‘The mechanism of frost action in concrete’, Stanton Walker Lecture No 3, Silver Springs, Md. National Sand and Gravel Association/National Ready Mixed Concrete Association, (1965)

[13] Liu ‘Frost deterioration in concrete due to deicing salt exposure: Mechanism, Mitigation and conceptual surface scaling model’, PhD University of Michigan,(2014)

[14] Sun and Scherer, ‘Effect of Air Voids on the Dilatation of Mortar During Freezing’, p. 896-901 in Poromechanics IV, Proc. Fourth Biot Conf. on Poromechanics, New York, 2009. eds. H.I. Ling, A. Smyth, R. Betti (DEStech Publications, Lancaster, PA, 2009)

[15] Teddy Fen-Chong et al (2013) Poroelastic Analysis of Partial Freezing in Cohesive Porous Materials, Journal of Applied Mechanics, MARCH 2013, Vol. 80 / 020910-1